

学位論文（要約）

Frontogenesis and frontolysis

in the Agulhas Return Current region

（アガラス反転流域の水温前線の強化・緩和過程）

平成 28 年 12 月博士（理学）申請

東京大学大学院理学系研究科

地球惑星科学専攻

大石 俊

Abstract

In mid-latitudes, it has long been considered that the atmosphere forces sea surface temperature (SST) variations, while oceanic effects on the atmosphere are negligible. However, with the recent advance of satellite observations and numerical models, substantial impacts of SST fronts on the overlying atmosphere in the western boundary currents and their extension regions have been revealed. Nevertheless, a fundamental question of how these SST fronts are reinforced and relaxed remains to be answered. Therefore, this thesis is devoted to quantitative understanding of frontogenesis and frontolysis processes of the SST front in the Agulhas Return Current (ARC) region in the southwestern Indian Ocean, where monsoonal wind influences are relatively weak and air-sea interaction associated with the SST front can be detected more easily.

From observational data analysis, it is found that the SST front in the ARC region is located around 45° – 40° S in 10° – 70° E and its latitudinal position is relatively stable in 40° – 70° E. Its intensity is 4 – $5^{\circ}\text{C } 100\text{km}^{-1}$, and undergoes a seasonal variation with slightly weaker (stronger) intensity in austral summer (winter). Through mixed layer temperature (MLT) balance analysis, it is shown that the SST front is maintained throughout the year owing to the balance between frontolysis by surface net heat flux

(NHF) and frontogenesis by oceanic processes.

Detailed analysis of the NHF reveals that larger (smaller) latent heat release on the northern (southern) side is due to larger (smaller) air-sea specific humidity difference. More specifically, the SST front causes a large meridional difference in surface saturated humidity across the front, while the air specific humidity gradient is reduced by meridional humidity advection associated with the passage of atmospheric disturbances.

Interestingly, the frontolysis by the NHF is amplified (damped) through mixed layer processes in austral summer (winter). In austral summer, strong heating of the sea surface by shortwave radiation is partially offset by larger (smaller) latent heat release north (south) of the front. As a result, surface warming is weaker (stronger) on the northern (southern) side, and thus the NHF relaxes the SST front. At the same time, the weaker (stronger) surface warming leads to deeper (shallower) mixed layer in the northern (southern) region. This meridional gradient in mixed layer depth (MLD) enhances the frontolysis, because the thicker (thinner) mixed layer north (south) of the front is less (more) sensitive to surface warming. Furthermore, the frontolysis by the NHF is amplified by the seasonally thin MLD that is very sensitive to surface forcing. On the other hand, stronger (weaker) surface cooling on the northern (southern) side of the front in austral winter, which is mainly due to the larger (smaller) latent heat release, contributes to frontolysis. However, deeper (shallower) mixed layer induced by the stronger (weaker) surface cooling on the northern (southern) side is less (more) sensitive to surface cooling and suppresses the frontolysis. Since the seasonally thick MLD in winter is relatively inert against surface forcing, the frontolysis is weakened further.

Due to the insufficient number of velocity observations in the ocean interior, the frontogenesis by oceanic processes is only estimated as residual in the observational data analysis. For this reason, detailed mechanisms of the oceanic processes are then quantitatively investigated using outputs from a high-resolution coupled general circulation model (CGCM), the Community Earth System Model (CESM). It is confirmed that this model realistically simulates main features of the SST front, including intensity, location, seasonality, MLD, and frontogenesis/frontolysis.

Among the oceanic processes, the contribution from horizontal advection is dominant for the frontogenesis, while entrainment does not contribute much to frontogenesis/frontolysis. Although a southward (northward) cross-isotherm flow north (south) of the front is weaker than a strong eastward along-isotherm current in the frontal region, this cross-isotherm confluent flow advects warmer (cooler) temperature toward the SST front on the northern (southern) side and plays the dominant role in the frontogenesis. In addition, the stronger (weaker) frontogenesis in austral summer (winter) is attributed to the stronger (weaker) cross-isotherm confluent flow, which may be linked to seasonal variations of the Agulhas Current, ARC, and Antarctic Circumpolar Current. On the other hand, the contribution from the entrainment is relatively small, because frontolysis by the larger (smaller) entrainment velocity on the northern (southern) side opposes frontogenesis by less (more) effective cooling associated with the thicker (thinner) mixed layer and smaller (larger) temperature difference between the mixed layer and entrained water in the northern (southern) region.

To gain further insight into the mean cross-isotherm confluent flow around the SST front, vorticity balance is examined. It is shown that anticyclonic (cyclonic)

vorticity advection north (south) of the front by the cross-isotherm confluence is in balance with the sum of cyclonic (anticyclonic) eddy cross-isotherm and mean along-isotherm vorticity advections.

Table of Contents

Abstract	i
Table of Contents	v
1 General introduction	1
1.1 Air-sea interaction in mid-latitudes	2
1.2 Frontogenesis and frontolysis in idealized models	3
1.3 The SST front in the Agulhas Return Current region	4
1.4 Purpose of this study	6
Figures	8
2 Frontolysis by surface heat flux in the Agulhas Return Current region with a focus on mixed layer processes	13
2.1 Introduction	14
2.2 Observational data and methodology	15
2.2.1 Observational data	15

2.2.2 Methodology	16
2.3 Frontogenesis/Frontolysis of the Agulhas Return Current Front	18
2.3.1 Frontogenesis/Frontolysis due to the NHF and MLD gradient	18
2.3.2 Causes of the MLD and NHF gradient	21
2.3.3 Seasonality of the NHF and MLD gradient term	25
2.4 Conclusions	27
Figures	30
3 Frontogenesis in the Agulhas Return Current region simulated by a high-resolution CGCM	45
4 General conclusions	46
4.1 Summary	47
4.2 Concluding remarks	50
Figure	56
Acknowledgements	57
References	59

Chapter 1

General introduction

1.1 Air-sea interaction in mid-latitudes

Air-sea interaction in mid-latitudes has attracted much attention because of its large impact on the climate system. It has been recognized that mid-latitude atmospheric variability causes sea surface temperature (SST) anomalies (e.g. Frankignoul 1985; Kushnir et al. 2002) through changes in turbulent heat fluxes (Cayan 1992), Ekman transport (Yasuda and Hanawa 1997), and entrainment at the base of the mixed layer (Miller et al. 1994). However, with the development of satellite observations and high-resolution general circulation models (GCMs), the importance of the oceanic influence on the atmosphere was highlighted in western boundary currents and their extension regions, where SST fronts and associated large amounts of heat release are found (e.g. Nonaka and Xie 2003; Xie 2004; Minobe et al. 2008).

Three mechanisms have been proposed for the oceanic impacts. First, the “vertical mixing mechanism” (Wallace et al. 1989; Xie et al. 1998; Chelton et al. 2004; Takatama et al. 2012, 2015) explains that over warmer (cooler) SSTs where the static stability is lower (higher), surface winds are accelerated (decelerated) due to intensified (weakened) turbulent mixing in the atmospheric boundary layer. Second, high SSTs on the equatorward side of an SST front result in sea level pressure (SLP) minima and rising air throughout the troposphere. This is known as the “pressure adjustment mechanism” (Lindzen and Nigam 1987; Feliks et al. 2004; Minobe et al. 2008, 2010; Shimada and Minobe 2011; Takatama et al. 2012, 2015). Finally, the “oceanic baroclinic adjustment” (Nakamura et al. 2008; Nonaka et al. 2009; Sampe et al. 2010, 2013; Ogawa et al. 2012) demonstrates that an SST front restores the meridional gradient of surface air temperature relaxed by atmospheric disturbances to its original condition through air-sea sensible heat flux exchange and thus fixes the storm track

position through the maintenance of atmospheric baroclinicity. Hence, an SST front plays an essential role in the air-sea interaction over western boundary currents and their extension regions.

For the above reasons, western boundary currents and their extension regions are now recognized as the key regions for air-sea interaction in mid-latitudes where the atmosphere affects the ocean and SST fronts have substantial impacts on the atmosphere. Therefore, understanding how SST fronts are reinforced and relaxed is essential for comprehensive understanding of air-sea interaction in mid-latitude regions. In this study, frontogenesis (frontolysis) is defined as reinforcement (relaxation) processes of the horizontal gradient of temperature over frontal regions.

1.2 Frontogenesis and frontolysis in idealized models

Past studies on frontogenesis are mostly based on idealized models. First, studies of atmospheric frontogenesis using idealized models that incorporate a horizontally barotropic confluent flow (Hoskins 1971; Hoskins and Bretherton 1972) are extended to the oceanic frontogenesis (MacVean and Woods 1980; Thompson 2000). These models with the confluent flow was able to simulate an instantaneous front, but discontinuity tended to be formed in a finite time due to the absence of frontolysis processes to balance with the frontogenesis.

Also, idealized models in which a flow with potential to cause baroclinic instability is incorporated are used (Samelson 1993; Wang 1993; Samelson and Chapman 1995; Spall 1995). These studies were motivated by intensive aircraft, ship, and mooring observations in the Gulf Stream region in 1984–86, called Frontal Air-Sea Interaction Experiment (FASINEX; Weller 1991; Pollard and Regier 1992), which

succeeded in obtaining detailed structure of the oceanic front. They demonstrated that frontogenesis occurs with evolutions of eddies and baroclinic waves through energy conversion from potential energy to eddy kinetic energy.

Furthermore, a flow with potential to cause barotropic instability is applied to the western boundary in idealized models (Waterman and Jayne 2011; Waterman and Hoskins 2013). They reproduce a time-mean jet and a pair of counterrotating recirculation gyres at the flank of the jet and suggested that eddies have roles in driving the mean jet and recirculation through influences on the speed and direction of the mean velocity (Hoskins 1983; Cronin 1996). Moreover, their sensitivity experiments demonstrated that the mean jet and recirculation are stronger (weaker) when the jet applied at the western boundary is stronger (weaker).

Therefore, frontogenesis in the ocean has been mostly investigated by incorporating frontogenetic flows into idealized models. This leaves us a question: how actually frontogenesis and frontolysis balance and SST fronts are maintained in the real world? This has not been investigated quantitatively, partly because of lack of high-resolution observational datasets and outputs from oceanic GCMs (OGCMs) that sufficiently resolve SST fronts. Recent progress of global observations in the ocean interior using temperature/salinity profiling floats known as Argo floats and numerical simulations with high-resolution OGCMs allows us to examine frontal scale ocean variability and associated air-sea interaction.

1.3 The SST front in the Agulhas Return Current region

As shown in Fig. 1.1, SST fronts are found in western boundary currents and their extension regions such as the Kuroshio and Kuroshio Extension, the Gulf Stream

(e.g. Kelly et al. 2010; Kwon et al. 2010), the Agulhas Return Current (ARC; e.g. Lutjeharms and Ansorge 2001; Lutjeharms 2006), and the Brazil–Malvinas Confluence (e.g. Saraceno et al. 2004; Tokinaga et al. 2005). In this study, the focus is on the SST front associated with the ARC in the southwestern Indian Ocean. This is because the SST front is away from the African continent and not strongly influenced by monsoonal winds. As a result, it is ideal for studying air-sea interaction associated with an SST front and this is one of the main reasons why the meridional SST profile of the southwestern Indian Ocean has been frequently used for idealized aqua-planet experiments targeting on this topic (Nakamura et al. 2008; Sampe et al. 2010, 2013; Ogawa et al. 2012). The results obtained in this thesis are thus expected to advance our understanding of mid-latitude ocean-atmosphere interaction.

The Agulhas Current flows poleward along the east coast of South Africa (Fig. 1.2). After retroflection of the Agulhas Current south of the African Continent around [20°E, 40°S], the ARC flows eastward to around [70°–80°E, 45°S] (Lutjeharms and Ansorge 2001; Boebel et al. 2003; Lutjeharms 2006; Beal et al. 2011). The Antarctic Circumpolar Current (ACC) flows eastward south of the ARC around [20°–30°E, 50°S], and then merges with the ARC around [40°E, 45°–40°S]. As a result, strong eastward currents distributed in 40°–70°E are associated with a strong SST front throughout the year (Fig. 1.3; Nakamura and Shimpo 2004). Hereafter, this front is called the ARC Front in this study.

The SST front has been shown to influence the atmospheric field using observations (O’Neill et al. 2005, 2010; Shimada and Minobe 2011) and a high-resolution coupled GCM (CGCM; Nonaka et al. 2009). In addition, the SST front is suggested to influence the storm track activity, whose variation affects the subtropical

high in the South Indian Ocean called the Mascarene High (Fig. 1.4; Miyasaka and Nakamura 2010; Morioka et al. 2015; Ohishi et al. 2015). In austral summer, variations in this high induce the northeast-southwest oriented dipole SST anomalies in the South Indian Ocean and rainfall anomalies over southern Africa (Fig. 1.5). This climate mode is known as the Indian Ocean Subtropical Dipole (IOSD; Behera and Yamagata 2001; Fauchereau et al. 2003; Suzuki et al. 2004; Hermes and Reason 2005; Chiodi and Harrison 2007; Morioka et al. 2010, 2012, 2013). The SST anomaly in the southwestern pole may influence the SST front in the ARC region as well as the Mascarene High due to changes in the storm track activity as mentioned above. Therefore, air-sea interaction over the ARC Front may play an active role in the ocean-atmosphere system of the South Indian Ocean through its influences on the storm track activity.

1.4 Purpose of this study

As described above, air-sea interaction in mid-latitudes has attracted interest and the influences of the SST fronts on the atmosphere are being clarified. However, the detailed mechanisms of frontogenesis/frontolysis of the SST fronts in the western boundary currents and their extension regions, an important factor in the air-sea interaction, have not been fully understood. Heat budget analysis within a mixed layer in frontal regions enables us to quantitatively investigate them. Here, the mixed layer is a surface layer with vertically uniform density, and mixed layer temperature (MLT) is determined by horizontal advection, surface net heat flux (NHF), entrainment, and horizontal/vertical diffusion. In this analysis, mixed layer depth (MLD) is also an important factor for the MLT, because MLD determines the sensitivity of the mixed layer to the NHF and entrainment. The recent progress of more dense observations in

the ocean interior by the Argo floats and high-resolution OGCMs allows us to perform the heat budget analysis within the mixed layer in frontal regions. Therefore, in this thesis, frontogenesis/frontolysis in the ARC region is investigated using high-resolution observational datasets and outputs from a CGCM, for gaining better understanding of air-sea interaction in mid-latitudes.

This thesis is organized as follows. In the next chapter, main characteristics of the ARC Front and its frontogenesis/frontolysis are discussed using observational datasets. In particular, dominant frontolysis processes that the NHF strongly (weakly) relaxes the front through mixed layer processes in austral summer (winter) are described quantitatively. In Chapter 3, using outputs from a high-resolution CGCM, the Community Earth System Model (CESM; Hurrell et al. 2013; Small et al. 2014), which realistically reproduces the SST front and MLD in the ARC region, we investigate detailed mechanisms of frontogenesis/frontolysis by oceanic processes, which are estimated as residual in Chapter 2. It is shown that stronger (weaker) confluence is the key to the stronger (weaker) frontogenesis in austral summer (winter). The final chapter summarizes the main results and discusses the implication of this study.

Figures

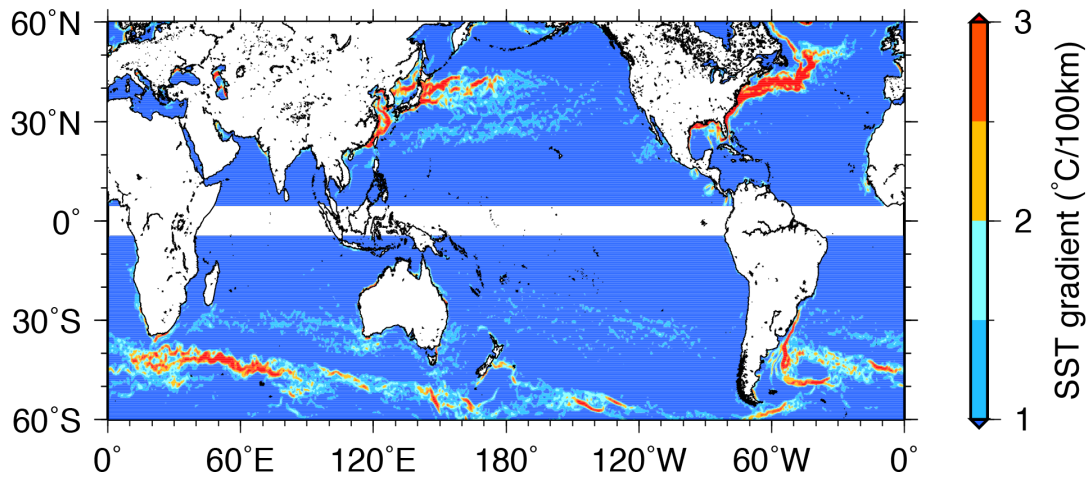
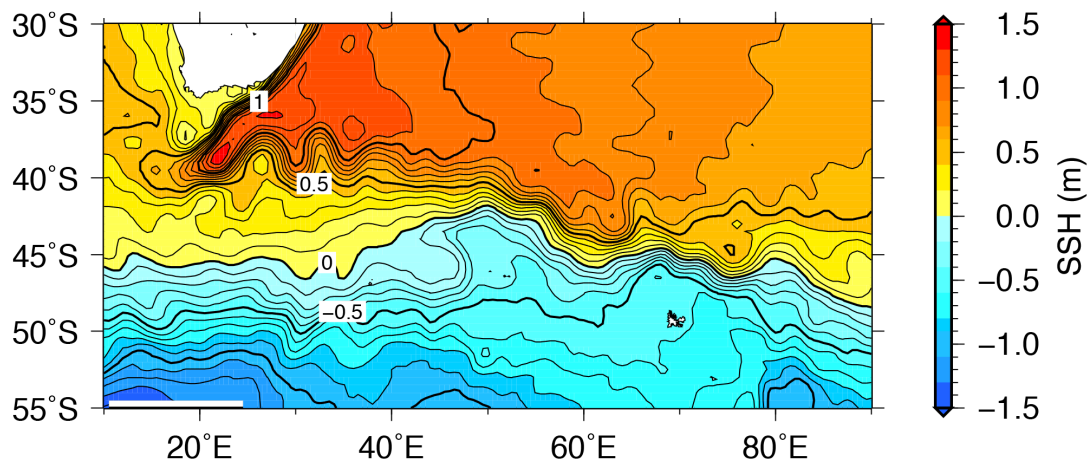


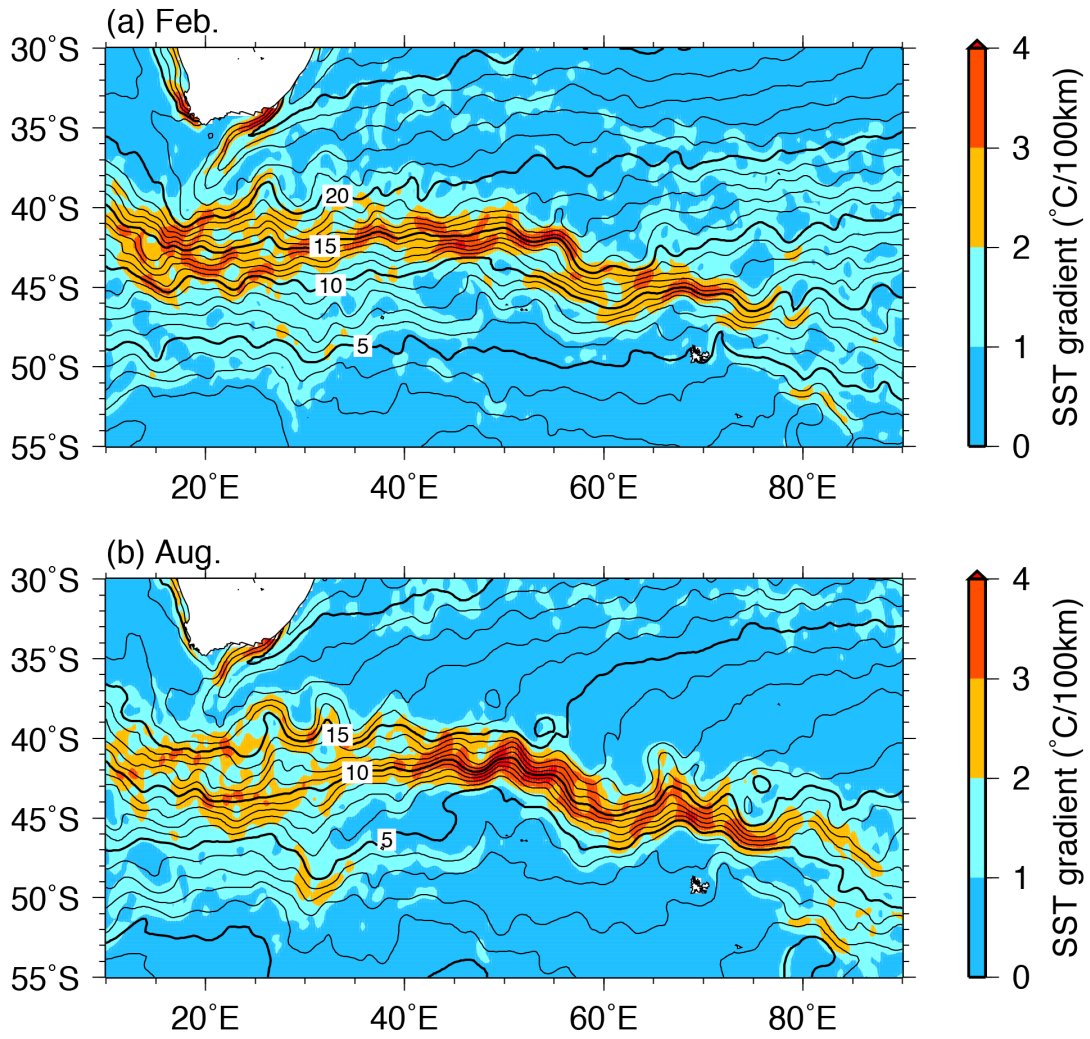
Fig. 1.1 Monthly climatology of horizontal sea surface temperature (SST) gradient for February (August) in the Northern (Southern) Hemisphere. Monthly-mean SST for 2003–2008 is obtained from Advanced Very High Resolution Radiometer (AVHRR) and Advanced Microwave Scanning Radiometer on the Earth Observing System (AMSR-E) Optimum Interpolation SST (AVHRR+AMSR OISST; Reynolds et al. 2007)



1

2 **Fig. 1.2** Mean sea surface height (SSH) in 2003–2008 obtained from Archiving
 3 Validation, and Interpretation of Satellite Oceanographic data (AVISO; Ducet et al.
 4 2000). Thin (Thick) contour intervals are 0.1 (0.5) m

5



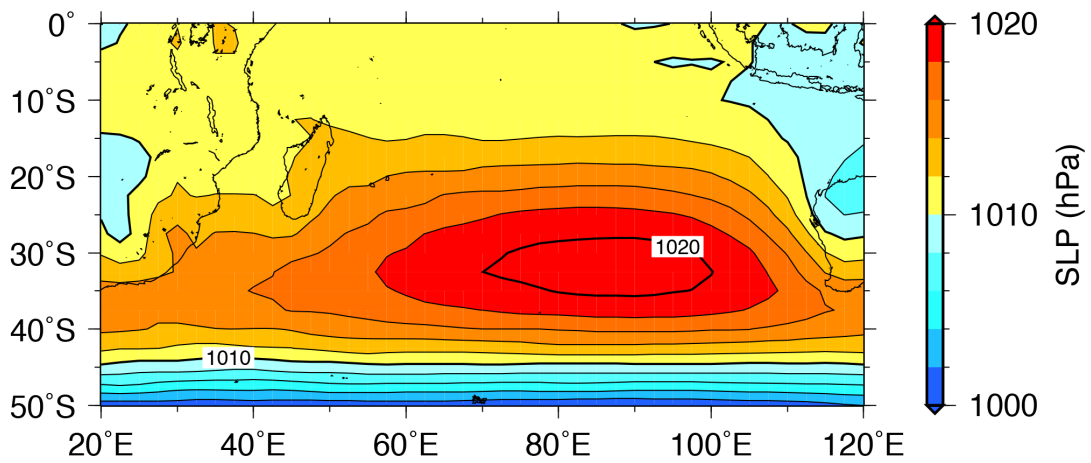
6

7 **Fig. 1.3** Monthly climatology of the SST gradient (color) and SST (contour) in a

8 February and **b** August from the AVHRR+AMSR OISST for the 2003–2008 period.

9 Thin (Thick) contour intervals are 1 (5) °C

10



11

12 **Fig. 1.4** Climatology of sea level pressure (SLP) in November–January obtained from
 13 the National Centers for Environmental Prediction–National Center for Atmospheric
 14 Research (NCEP–NCAR) reanalysis 1 (Kalnay et al. 1996) for the period of 1951–2012.

15 Thin (Thick) contour intervals are 2 (10) hPa. Reprinted from Ohishi et al. (2015). With
 16 permission of Springer

17

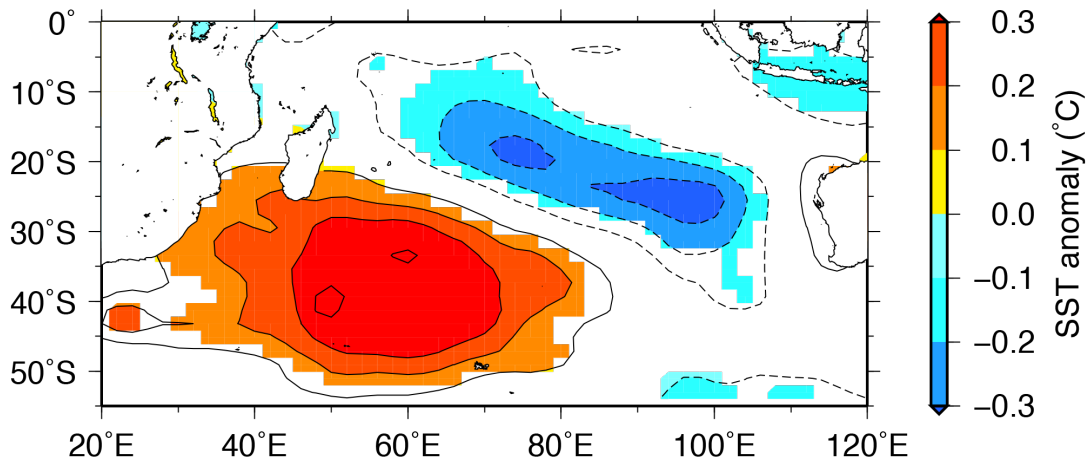


Fig. 1.5 Regression coefficients between the Indian Ocean Subtropical Dipole (IOSD) index and SST anomalies. Anomalies significant at the 99% confidence level by the two-tailed t-test are shaded. Contour intervals are 0.1°C and positive (negative) values are represented by solid (dashed) contour lines. The IOSD index is the standardized time coefficient of the second empirical orthogonal function (EOF) mode for austral summer (December–February) SST anomalies in the South Indian Ocean [20° – 120°E , 55°S – 0°] (Ohishi et al. 2015). Note that the first EOF mode represents warming tendency in the South Indian Ocean. Extended Reconstructed SST (ERSST; Smith et al. 2008) version 3b for 1951–2012 is used. Reprinted from Ohishi et al. (2015). With permission of Springer

Chapter 2

Frontolysis by surface heat flux in the Agulhas Return Current region with a focus on mixed layer processes

This chapter has been published as:

Ohishi S, Tozuka T, Komori N (2016) Frontolysis by surface heat flux in the Agulhas Return Current region with a focus on mixed layer processes: Observation and a high-resolution CGCM. *Clim Dyn* 47: 3993–4007. doi:10.1007/s00382-016-3056-0

2.1 Introduction

As described in the previous chapter, recent progress of the global observations in the ocean interior enables us to perform a heat budget analysis within a mixed layer in frontal regions. Tozuka and Cronin (2014) examined the frontogenesis/frontolysis in the Agulhas Return Current (ARC) region using observational datasets. As seen in Figs. 2.1a, b, smaller (larger) surface warming in austral summer and larger (smaller) surface cooling in austral winter are found north (south) of the ARC Front. Thus, the surface net heat flux (NHF) tends to relax the front if the mixed layer depth (MLD) were constant across the sea surface temperature (SST) front. However, they noticed that the MLD is deeper (shallower) to the north (south) of the front in the ARC region (Figs. 2.1c, d). In addition, they revealed that the frontolysis by the NHF is amplified (damped) in austral summer (winter) owing to deeper mixed layer on the northern side of the SST front, but the causes of the meridional MLD gradient were not examined in detail. Thus, we investigate the causes of the MLD gradient and seasonal dependence of the frontolysis by the NHF using observational datasets in this chapter.

This chapter is organized as follows. A brief description of observational data and methodology used in this chapter is given in Section 2.2. Section 2.3 describes the main features of the SST front associated with the ARC, and discusses the frontogenesis/frontolysis and causes of the MLD and NHF gradient including their seasonal dependence using observational data. Conclusions are given in the final section.

2.2 Observational data and methodology

2.2.1 Observational data

We use monthly-mean sea surface temperature (SST) from Advanced Very High Resolution Radiometer (AVHRR) and Advanced Microwave Scanning Radiometer on the Earth Observing System (AMSR-E) Optimum Interpolation SST (AVHRR+AMSR OISST; Reynolds et al. 2007) on 0.25° longitude \times 0.25° latitude grid. Monthly surface heat fluxes, specific humidity at 2 m, and wind speed at 10 m are adopted from the Objectively Analyzed air-sea Fluxes (OA Flux; Yu and Weller 2007). We estimate surface saturated specific humidity using monthly SST from the OA Flux and sea level pressure (SLP) from the ERA-interim global atmospheric reanalysis (Dee et al. 2011) produced by the European Centre for Medium-Range Weather Forecasts (ECMWF) by applying the Coupled Ocean-Atmosphere Response Experiment (COARE) version 3.0 flux algorithm (Fairall et al. 2003). The daily wind and air specific humidity, saturated specific humidity at the surface, and heat fluxes from Japanese Ocean Flux Data sets with Use of Remote Sensing Observations version 2 (J-OFURO2; Kubota et al. 2002) and the Japanese 55-year Reanalysis (JRA-55; Kobayashi et al. 2015) are also used, and we have confirmed that the obtained results are almost the same with those of the OA Flux. The OA Flux, ERA-interim, and J-OFURO2 have a horizontal resolution of $1^\circ \times 1^\circ$, and JRA-55 has 1.125° longitude \times 1.125° latitude grid. The analysis period is from January 2003 to December 2008, because spurious jumps in the intensity of the SST front in the ARC region are detected in the AVHRR-only OISST (figure not shown). It may be due to changes in the observation satellites (Reynolds et al. 2007; Masunaga et al. 2015) and/or clouds and

aerosols around the mid-latitude jet that hamper SST measurements (Chelton and Wentz 2005). We use the monthly temperature climatology from Monthly Isopycnal/Mixed-layer Ocean Climatology (MIMOC; Schmidt et al. 2013), which is mainly based on the Argo float profiles during 2007–2011 and has 0.5° longitude \times 0.5° latitude grid with 81 vertical levels and resolves main features of SST fronts. The bottom topography from the 5-min Earth Topography (ETOPO5) dataset is adopted.

2.2.2 Methodology

To quantitatively investigate the causes of the MLD gradient, we use two diagnostic equations. One is the energetic equation for estimating the entrainment velocity w_e :

$$\frac{1}{2} \alpha g H \Delta T w_e = m_0 u_*^3 + \frac{\alpha g}{\rho_0 c_p} \int_{-H}^0 q_{sw}(z) dz - \frac{\alpha g H}{2 \rho_0 c_p} (Q_{net} + q_{sw}(-H)) - m_c \frac{\alpha g H}{4 \rho_0 c_p} (|Q_{net}| - Q_{net}) \quad (2.1)$$

(Niiler and Kraus 1977; Qiu and Kelly 1993). Here, α ($= 2.5 \times 10^{-4} \text{ }^\circ\text{C}^{-1}$) is the thermal expansion coefficient, g is the acceleration due to gravity, c_p ($= 3990 \text{ J kg}^{-1} \text{ }^\circ\text{C}^{-1}$) is the specific heat of the sea water, H is the MLD defined as a depth at which the temperature is $0.5 \text{ }^\circ\text{C}$ lower than the SST, and ΔT ($\equiv T_{mix} - T_{-H-20m}$) is the temperature difference between the mixed layer and entrained water. We use the water temperature at 20 m below the mixed layer base as the temperature of the entrained water following Yasuda et al. (2000) and Morioka et al. (2012). Note that the temperature used for estimating the MLD and the temperature difference is

interpolated at 5 m interval using the method of Akima (1970). Also, m_0 is a coefficient for the efficiency of wind stirring and we use $m_0 = 0.5$ (Davis et al. 1981). Frictional velocity u_* is defined by $u_* = \sqrt{\rho_a C_D u_{10}^2 / \rho_0}$, where ρ_a ($= 1.3 \text{ kg m}^{-3}$) is air density, ρ_0 ($= 1026 \text{ kg m}^{-3}$) is the density of the sea water, C_D ($= 1.5 \times 10^{-3}$) is a drag coefficient, and u_{10} is wind speed at 10 m. Downward shortwave radiation at depth z , $q_{sw}(z)$, is parameterized by

$$q_{sw}(z) = Q_{sw} \left\{ R \exp\left(\frac{z}{\gamma_1}\right) + (1 - R) \exp\left(\frac{z}{\gamma_2}\right) \right\} \quad (2.2)$$

(Paulson and Simpson 1977), where Q_{sw} is shortwave radiation at the sea surface, R ($= 0.58$) is a separation constant, and γ_1 ($= 0.35 \text{ m}$) and γ_2 ($= 23.0 \text{ m}$) are attenuation length scales. These values are set to the case of Type I (clear water) from Jerlov (1976). Also, Q_{net} is the NHF (positive values indicating heat flux into the ocean), m_c is a convective efficiency coefficient, and we adopt $m_c = 0.83$ (Deardorff et al. 1969). The entrainment velocity is assumed to vanish when it becomes negative. Each term on the right-hand side (RHS) of Eq. (2.1) represents the contribution from the wind stirring, incidence of shortwave radiation, and NHF, respectively. Although horizontal induction and vertical velocity are difficult to estimate from the observational data, as will be shown in Chapter 3 using outputs from a coupled general circulation model (CGCM), the entrainment velocity corresponds well with the MLD tendency in the ARC region.

When the entrainment velocity is zero, i.e., in a shoaling phase, the diagnostic equation for estimating the MLD is

$$H_m = \frac{m_0 u_*^3 + \frac{\alpha g}{\rho_0 c_p} \int_{-H_m}^0 q_{sw}(z) dz}{\frac{\alpha g}{2\rho_0 c_p} (Q_{net} + q_{sw}(-H_m))} \quad (2.3)$$

(Kraus and Turner 1967; Niiler and Kraus 1977; Qiu and Kelly 1993). Here, the diagnostic MLD, H_m , is called the Monin–Obukhov Depth (MOD). Equations (2.1) and (2.3) are useful when examining the relative importance of wind speed, shortwave radiation, and NHF in determining the entrainment velocity and the MLD, respectively. Since these diagnostic equations assume a horizontally uniform field, they may not be appropriate in frontal regions. However, the weak meridional velocity in the frontal region (less than about 5 cm s^{-1} as will be shown in Chapter 3) implies that transport of denser/lighter water across the front is small, and that the diagnostic equations can provide reasonable results around the ARC region.

2.3 Frontogenesis/Frontolysis of the Agulhas Return Current Front

2.3.1 Frontogenesis/Frontolysis due to the NHF and MLD gradient

In this study, the intensity and position of the SST front are defined by the maximum of the meridional SST gradient within $55^\circ\text{--}35^\circ\text{S}$ at each longitude and its latitude, respectively. Figures 2.2 shows their mean and standard deviation throughout the analysis period. The front with strong intensity of $4\text{--}5 \text{ }^\circ\text{C } 100\text{km}^{-1}$ is found in $20^\circ\text{--}70^\circ\text{E}$ and its meridional location is relatively stable; it lies around 42°S west of 55°E , but shifts southward and is found around 45°S from 60°E to 70°E . The frontal position may be influenced by the bottom topography (Fig. 2.3) (e.g. Chelton et al. 1990; Isoguchi et al. 2006; De Boer et al. 2013), although its detailed mechanism needs to be

investigated in a future study.

To investigate the seasonal variation of the ARC Front, we calculate the intensity averaged over 40°–50°E, where the meridional variation in the front is relatively small and its effects can be minimized in the subsequent analyses (Fig. 2.2a). The ARC Front undergoes a seasonal variation with the maximum of 5.3 °C 100km⁻¹ in June and the minimum of 4.3 °C 100km⁻¹ in December (Fig. 2.4). Thus, a remarkable SST front exists throughout the year in the ARC region, as has been pointed out by Nakamura and Shimpo (2004).

To understand the mechanism of the seasonal variation, we take the meridional derivative of the mixed layer temperature (MLT) balance equation (e.g. Qiu and Kelly 1993; Moisan and Niiler 1998) to obtain an equation for the rate of frontogenesis:

$$\frac{\partial}{\partial t} \left(\frac{\partial T_{mix}}{\partial y} \right) = \frac{\partial}{\partial y} \left(\frac{Q_{net} - q_{sw}(-H)}{\rho_0 c_p H} \right) + \frac{\partial}{\partial y} (\text{oceanic term}) \quad (2.4)$$

(Tozuka and Cronin 2014). Here, (*oceanic term*) includes the horizontal advection, entrainment, horizontal/vertical diffusion, and residual. To obtain the meridional gradient, we first calculate the monthly climatologies by taking an average in artificial boxes of 10° longitude × 4° latitude on both sides of the SST front in 40°–50°E, and then take their difference. We note that qualitatively the same results are obtained even when we have used 35°–50°E and 40°–45°E for the longitudinal extent and 3° and 5° for the latitudinal extent. As shown in Fig. 2.5, the rate of frontogenesis [the left-hand side (LHS) term of Eq. (2.4)] well explains the seasonal variation of the SST front

shown in Fig. 2.4. For all months, the ARC Front is weakened by the 1st term on the RHS of Eq. (2.4), denoted as the NHF/MLD gradient term in this study, while it is reinforced by the gradient of the oceanic term [the 2nd term on the RHS of Eq. (2.4)], which is calculated as the difference between the rate of frontogenesis and the NHF/MLD gradient term, because the number of the velocity observations in the ocean interior is insufficient. Moreover, the frontolysis (frontogenesis) by the former (latter) is stronger in austral summer and weaker in austral winter.

To quantitatively examine the role of the NHF and MLD gradient in the frontogenesis/frontolysis, the NHF/MLD gradient term is further decomposed as follows:

$$\frac{\partial}{\partial y} \left(\frac{Q_{net} - q_{sw}(-H)}{\rho_0 c_p H} \right) = \frac{1}{\rho_0 c_p H} \frac{\partial}{\partial y} (Q_{net} - q_{sw}(-H)) - \frac{Q_{net} - q_{sw}(-H)}{\rho_0 c_p H^2} \frac{\partial H}{\partial y}. \quad (2.5)$$

Here, the 1st (2nd) term on the RHS represents the contribution from the NHF (MLD) gradient. The NHF gradient term [the 1st term on the RHS of Eq. (2.5)] displays the dominant contribution to the NHF/MLD gradient term in all months (Fig. 2.6). This indicates that the weaker (stronger) surface warming (cooling) on the northern side during austral summer (winter) tends to relax the ARC Front, as shown in Figs. 2.1a, b, 2.7a. In contrast, the sign of the MLD gradient term [the 2nd term on the RHS of Eq. (2.5)] changes with seasons (Fig. 2.6). In austral summer, the MLD gradient term induces frontolysis, because the thicker mixed layer in the northern region is less sensitive to surface warming compared to the southern region (Figs. 2.1c, 2.7b). In particular, it is comparable to the NHF gradient term in November and December. In

contrast, it contributes to slight frontogenesis in austral winter, because the deeper mixed layer on the northern side of the front is less sensitive to surface cooling compared to the southern side (Figs. 2.1d, 2.7b). Thus, the MLD gradient enhances the frontolysis by the NHF gradient in austral summer, while it slightly suppresses the frontolysis in austral winter, as previously pointed out by Tozuka and Cronin (2014).

2.3.2 Causes of the MLD and NHF gradient

(a) Causes of the MLD gradient

Prior to investigating the causes of the MLD gradient in austral summer using the MOD [Eq. (2.3)], the MOD and observed MLD are compared in the northern and southern regions. Since the MOD can only be estimated when the mixed layer is in the shoaling phase due to its formulation, the MOD is calculated only in November and December when both regions are in the shoaling phase (northern and/or southern regions are not in the shoaling phase in January and February). As shown in Fig. 2.8, the MOD is in good agreement with the observed MLD. Also, the MOD (observed MLD) in the northern region is deeper by 64m (52m) in November and 39m (14m) in December compared to the southern region, and thus the MOD gradient corresponds well with the observed MLD gradient. This suggests that the MOD can be used to investigate the causes of the MLD gradient in the frontal region.

The meridional derivative of the MOD can be expressed as

$$\frac{\partial H_m}{\partial y} \equiv \frac{\partial}{\partial y} \left(\frac{u+q}{Q} \right) = \frac{1}{Q} \frac{\partial u}{\partial y} + \frac{1}{Q} \frac{\partial q}{\partial y} - \frac{u+q}{Q^2} \frac{\partial Q_{net}}{\partial y} - \frac{u+q}{Q^2} \frac{\partial q_{sw}(-H_m)}{\partial y}, \quad (2.6)$$

where u , q , and Q represents the term associated with the wind stirring, shortwave radiation, and NHF in Eq. (2.3), respectively. Here, each term on the RHS denotes the contribution from the meridional gradient of wind speed, incidence of shortwave radiation, NHF, and downward shortwave radiation at the base of the MOD, respectively. Among these four terms, the contribution from the NHF gradient has the dominant influence on the formation of the MOD gradient for both months (Fig. 2.9). This indicates that the weaker (stronger) surface warming in the northern (southern) region leads to the deeper (shallower) mixed layer, and thus results in the MLD gradient in austral summer.

The observed MLD gradient tends to increase from February and reaches its maximum in October (Fig. 2.7b). This implies that the entrainment velocity is larger on the northern side during austral winter. The diagnostic entrainment velocity and its gradient of Eq. (2.1) in both northern and southern regions are calculated only when both regions are in the deepening phase (i.e. March–August). Figure 2.10a shows that the diagnostic entrainment velocity is consistently larger on the northern side, in agreement with the increasing tendency of the observed MLD gradient (Fig. 2.7b).

To examine the causes of the meridional gradient in the entrainment velocity, we decompose the meridional derivative of Eq. (2.1) as follows:

$$\begin{aligned} \frac{\partial w_e}{\partial y} &\equiv \frac{\partial}{\partial y} \left(\frac{u + q + HQ}{H\Delta T} \right) \\ &= \frac{1}{H\Delta T} \frac{\partial u}{\partial y} + \frac{1}{H\Delta T} \frac{\partial q}{\partial y} + \frac{1}{\Delta T} \frac{\partial Q_{net}}{\partial y} + \frac{1}{\Delta T} \frac{\partial q_{sw}(-H)}{\partial y} \\ &\quad - \frac{u + q}{H^2\Delta T} \frac{\partial H}{\partial y} - \frac{u + q + HQ}{H\Delta T^2} \frac{\partial \Delta T}{\partial y}. \end{aligned} \quad (2.7)$$

Here, each term on the RHS represents the contribution from the meridional gradient of

the wind speed, incidence of shortwave radiation, NHF, downward shortwave radiation at the base of the mixed layer, MLD, and temperature difference, respectively. Figure 2.10b shows that the entrainment velocity gradient is mainly due to the NHF gradient. Thus, the stronger cooling leads to the deeper mixed layer in the northern region. In May and June, the temperature difference gradient also makes a substantial contribution to the entrainment velocity gradient. This is attributed to the fact that the smaller (larger) energy is required for entrainment, when the temperature difference is smaller (larger). The wintertime temperature difference is likely to be linked to the Mode Water formation process (e.g. Hanawa and Talley 2001; Tsubouchi et al. 2010; Oka and Qiu 2012); the vertically uniform layer is formed owing to the wintertime deep mixed layer. In contrast, the MLD gradient acts to relax the diagnostic entrainment velocity gradient, because the thicker mixed layer in the northern region becomes less sensitive to the energy input from the atmosphere. The meridional gradients of the wind speed and shortwave radiation make minor contributions.

Therefore, the MLD gradient that plays an important role in the frontolysis process is predominantly generated by the NHF gradient in both austral summer and winter. In austral summer, the weaker (stronger) surface warming north (south) of the front leads to deeper (shallower) MLD, while in austral winter, the stronger (weaker) surface cooling on the northern (southern) side induces the larger (smaller) entrainment velocity causing the deeper (shallower) MLD. How the meridional gradient in entrainment velocity contributes to the frontogenesis/frontolysis will be discussed in Chapter 3.

(b) *Causes of the NHF gradient*

The NHF gradient can be decomposed as

$$\frac{\partial Q_{net}}{\partial y} = \frac{\partial Q_{lh}}{\partial y} + \frac{\partial Q_{sh}}{\partial y} + \frac{\partial Q_{lw}}{\partial y} + \frac{\partial Q_{sw}}{\partial y}, \quad (2.8)$$

where Q_{lh} , Q_{sh} , and Q_{lw} denote latent heat flux, sensible heat flux, and longwave radiation, respectively. As is clear from Fig. 2.11, the gradient of latent heat flux is dominant among the four in all months.

For this reason, the latent heat flux gradient is further decomposed as follows:

$$\begin{aligned} \frac{\partial Q_{lh}}{\partial y} &\equiv \frac{\partial}{\partial y} (C u_{10} (q_s - q_a)) \\ &= C (q_s - q_a) \frac{\partial u_{10}}{\partial y} + C u_{10} \frac{\partial q_s}{\partial y} - C u_{10} \frac{\partial q_a}{\partial y} + (res). \end{aligned} \quad (2.9)$$

Here, $C = \rho_a C_e L$, where C_e is a transfer coefficient for latent heat and L is the latent heat of evaporation, q_s is 98% of surface saturated specific humidity depending primarily on SST, q_a is air specific humidity, and (res) is a residual term, which includes the contribution from the gradient of C and sub-monthly terms. Figure 2.12 indicates that the wind speed gradient and the residual term have minor effects on the formation of the meridional gradient of latent heat flux for all months, while the meridional gradient of surface saturated specific humidity is about twice as steep as that of air specific humidity.

To gain insight into the difference of these specific humidity gradients, daily latitude-time sections in July 2003 is displayed as an example in Fig. 2.13. Due to the

high storm track activity in the ARC region (e.g. Nakamura and Shimpo 2004; Nakamura 2012), it is found that strong southwesterly winds occasionally blow with the passage of atmospheric disturbances. Since it appears that the meridional winds advect air with lower (higher) air specific humidity from the southern (northern) to northern (southern) side, we estimate the meridional air specific humidity flux $\overline{v'q_a'}$, where v denotes surface meridional wind, the prime terms represent the difference between the daily and monthly values, and the overbar means monthly mean (Fig. 2.14). Since the negative air humidity flux is distributed over the SST front, it is suggested that the meridional advection of air specific humidity induces smaller air specific humidity in the frontal region. On the other hand, the surface saturated specific humidity does not change much due to the large oceanic heat capacity. Consequently, larger (smaller) difference between the surface saturated and air specific humidity is formed on the northern (southern) side, and thus larger (smaller) amount of the latent heat is released.

In contrast to the latent heat flux gradient, the shortwave radiation gradient has small positive values in all months, and does not contribute much to NHF gradient. This shortwave radiation gradient suggests that the latitudinal dependence is dominant, but recent ship observations reported that low-level clouds on the warmer side of SST fronts reduce downward shortwave radiation reaching the sea surface (Kawai et al. 2015). Since observations and simulations have uncertainty in shortwave radiation around SST fronts, an accurate estimation of shortwave radiation gradient awaits further studies.

2.3.3 Seasonality of the NHF and MLD gradient term

In this subsection, we discuss why stronger (weaker) frontolysis by the NHF

gradient term and frontolysis (weak frontogenesis) by the MLD gradient term occurs in austral summer (winter), as shown in Fig. 2.6. The NHF gradient undergoes a relatively small seasonal variation (Fig. 2.11), while the MLD in the northern and southern regions shows large seasonal variations with shallow (deep) MLD in austral summer (winter) (Figs. 2.1c, d, 2.7b). Thus, the seasonality of the frontolysis by the NHF gradient term in Eq. (2.5) mainly stems from the seasonal variation of the MLD.

To investigate the causes of the seasonality in the MLD gradient term in Eq. (2.5), this term is rearranged as follows:

$$-\frac{Q_{net} - q_{sw}(-H)}{\rho_0 c_p H^2} \frac{\partial H}{\partial y} = \frac{Q_{net} - q_{sw}(-H)}{\rho_0 c_p H} \times \left(-\frac{1}{H} \frac{\partial H}{\partial y} \right). \quad (2.10)$$

Here, the 1st part of the RHS represents the effect of heat flux on the MLT tendency, while the 2nd part indicates the MLD gradient standardized by the MLD averaged across the SST front in the northern and southern regions. The relatively thin mixed layer in November and December compared to austral winter amplifies the effect of heat flux due to smaller heat capacity (i.e. the 1st part becomes larger) (Figs. 2.1c, d, 2.7b, c). Also, the effect of the MLD gradient becomes larger owing to relatively thin mixed layer (i.e. the 2nd part becomes larger) (Fig. 2.7c). As a result, relatively strong frontolysis by the MLD gradient takes place (Fig. 2.6). From January to March, in spite of the very thin mixed layer (Fig. 2.7b), only very weak frontolysis by the MLD gradient term occurs due to the very small MLD gradient. This is because the change in the MLD becomes smaller as the surface warming becomes stronger [as is clear from the fact that Q is found in the denominators of all terms on the RHS of Eq. (2.6)]. In

addition, the earlier onset of the deepening phase in the southern region (Fig. 2.7b) may also contribute to the decrease in the MLD gradient. From April to July, although the strong surface cooling occurs (Fig. 2.7a), the MLD gradient term induces only slight frontogenesis (Fig. 2.6). This is because the relatively thick mixed layer results in the smaller effect of heat flux and the MLD gradient compared to the relatively thin mixed layer in November and December (i.e. the 1st and 2nd parts become smaller) (Figs. 2.1c, d, 2.7b, c). During August–October, the frontogenesis/frontolysis becomes very weak because of the deep MLD and the small NHF. Thus, the seasonality in frontogenesis/frontolysis due to the MLD gradient term primarily depends on that in the MLD.

2.4 Conclusions

A clear SST front, defined as the maxima of the meridional SST gradient within the latitudinal band of 55° – 35° S, extends from 20° E to 70° E in the southwestern Indian Ocean and shows only small meridional variations within 40° – 70° E. In this study, we have first investigated the seasonal variation of the ARC Front in 40° – 50° E using observational datasets. It is shown that oceanic processes tend to reinforce the ARC Front, while the NHF acts as the frontolysis process throughout the year. Figure 2.15 displays schematic diagrams summarizing the influence of the NHF on the frontogenesis/frontolysis through mixed layer processes in austral summer and winter. The ARC Front forms the stronger meridional gradient of surface saturated specific humidity, while the meridional advection of air specific humidity associated with the passage of atmospheric disturbances induces the weaker air specific humidity gradient. Consequently, due to larger (smaller) air-sea specific humidity difference on the

northern (southern) side of the front, latent heat release is larger (smaller) throughout the year.

In austral summer (Fig. 2.15a), this results in smaller (larger) positive NHF on the northern (southern) side and thus relaxes the SST front. At the same time, weaker (stronger) surface warming leads to deeper (shallower) mixed layer. This enhances the frontolysis, because the thicker (thinner) mixed layer is less (more) sensitive to surface warming. Therefore, the latent heat flux gradient, which is generated by the SST front through the formation of the meridional gradient in surface saturated specific humidity, strongly relaxes the SST front due to its impact on both the NHF and the MLD. In addition, the above effects are amplified by the seasonally thin mixed layer.

In austral winter (Fig. 2.15b), the larger (smaller) latent heat release results in the stronger (weaker) surface cooling on the northern (southern) side and contributes to the frontolysis. However, only weak frontolysis occurs in winter owing to the seasonally much deeper mixed layer. Furthermore, the stronger (weaker) surface cooling on the northern (southern) side induces larger (smaller) entrainment velocity. The resulting deeper (shallower) mixed layer tends to strengthen the front in contrast to summer, because the thicker (thinner) mixed layer on the northern (southern) side is less (more) sensitive to surface cooling. Thus, the frontolysis by the NHF in austral winter is less prominent compared to summer owing to the seasonally deep mixed layer and the meridional MLD gradient caused by the NHF gradient.

This chapter clearly shows that the frontolysis by the NHF is not merely a process at the sea surface as previously thought, but involves mixed layer processes, and that the meridional variation in MLD across the ARC Front plays an important role. Although this effect had been pointed out by Tozuka and Cronin (2014), we have

quantitatively discussed the mechanisms of the meridional variation in the MLD for the first time, and provided details of the seasonal variation in the frontolysis. On the other hand, details of the oceanic processes and causes of their seasonal variation need to be investigated for more comprehensive understanding of the ARC Front. Due to the insufficient number of velocity observations in the ocean interior, it is difficult to accurately quantify oceanic processes using observational datasets. Consequently, using a high-resolution CGCM, frontogenesis by oceanic processes in the ARC region is investigated quantitatively in the next chapter.

Figures

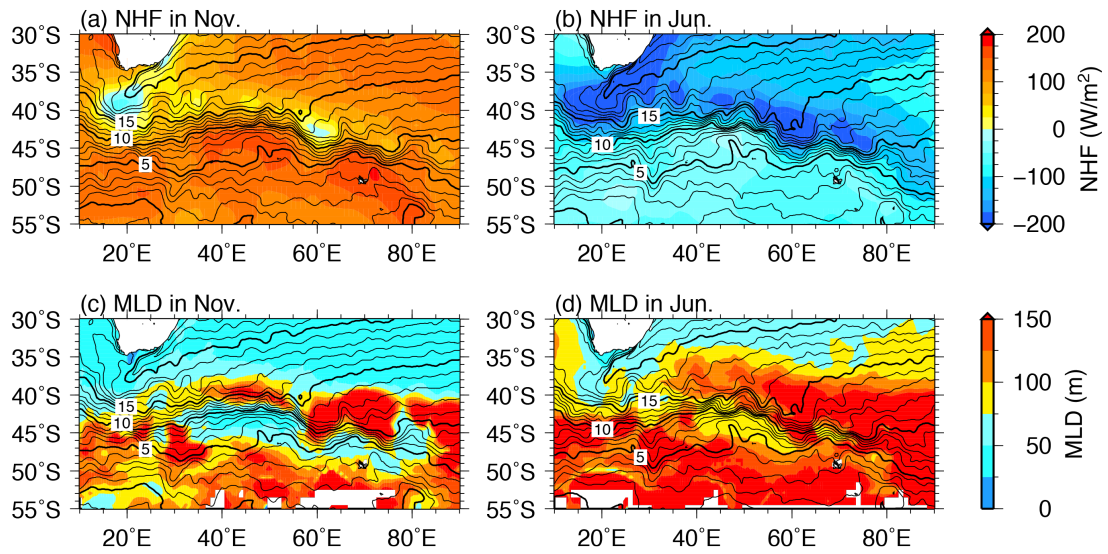


Fig. 2.1 Climatology of the surface net heat flux (NHF; positive values indicating heat flux into the ocean) in **a** November and **b** June. Contours indicate sea surface temperature (SST) climatology. Thin (Thick) contour intervals are 1 (5) °C. **c, d** As in **(a)** and **(b)**, but for mixed layer depth (MLD). With permission of Springer

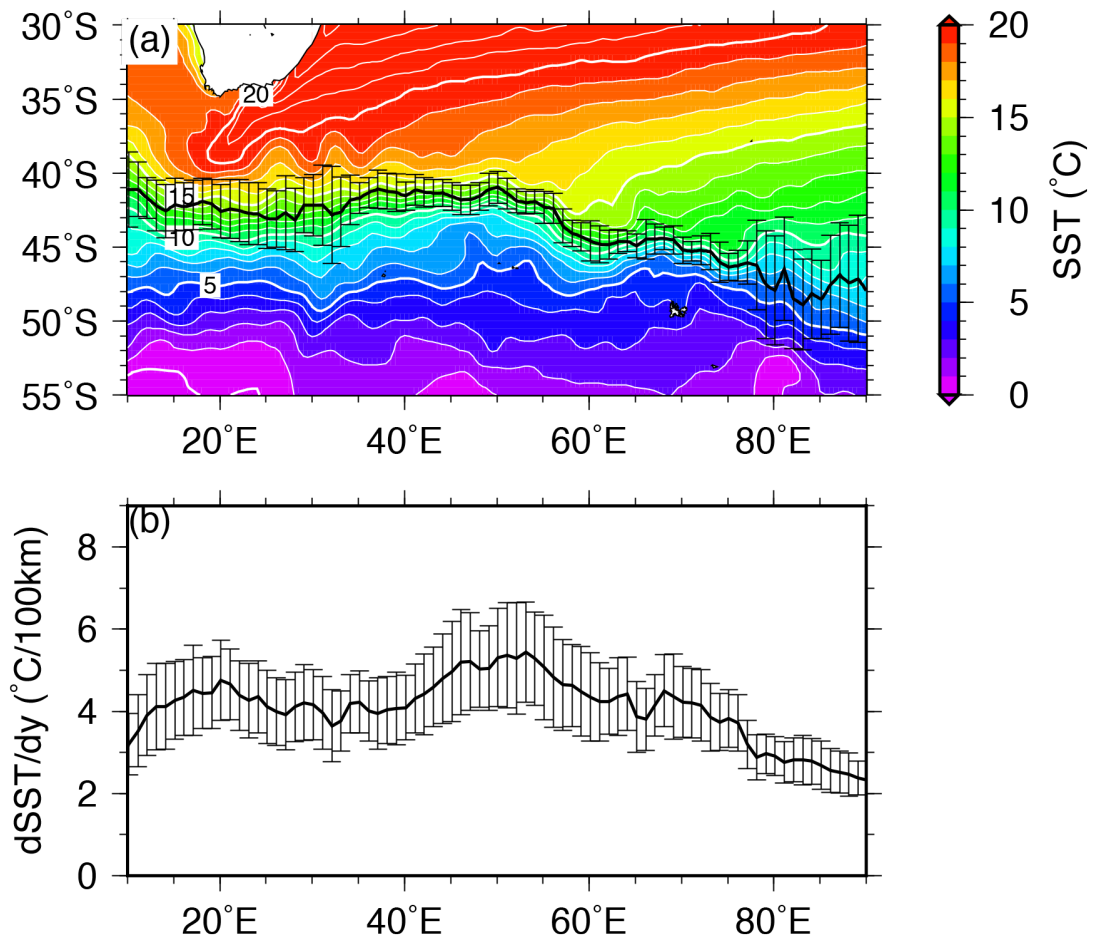


Fig. 2.2 Annual mean of the **a** position and **b** intensity of the SST front. Error bars denote the standard deviation over the analysis period. In **(a)**, color and white contours represent SST climatology. Thin (Thick) contour intervals are 1 (5) °C. With permission of Springer

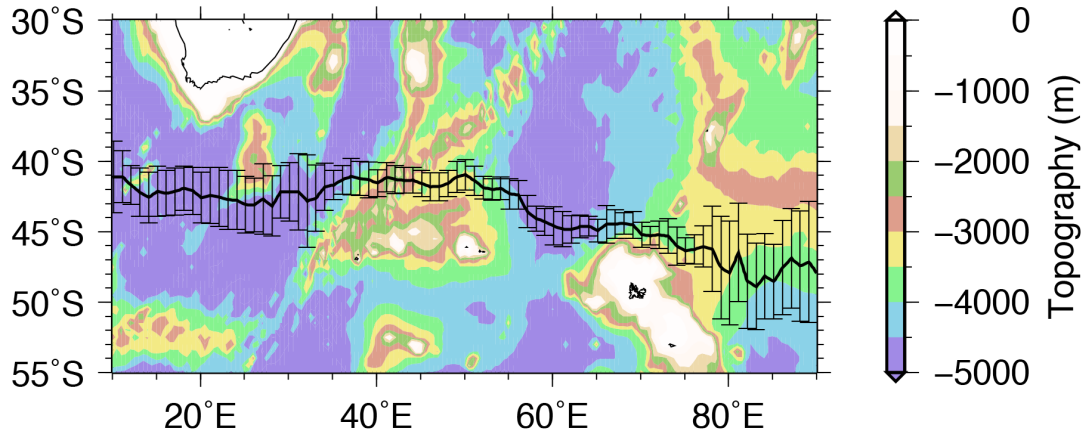


Fig. 2.3 As in Fig. 2.2a, but color represents topography

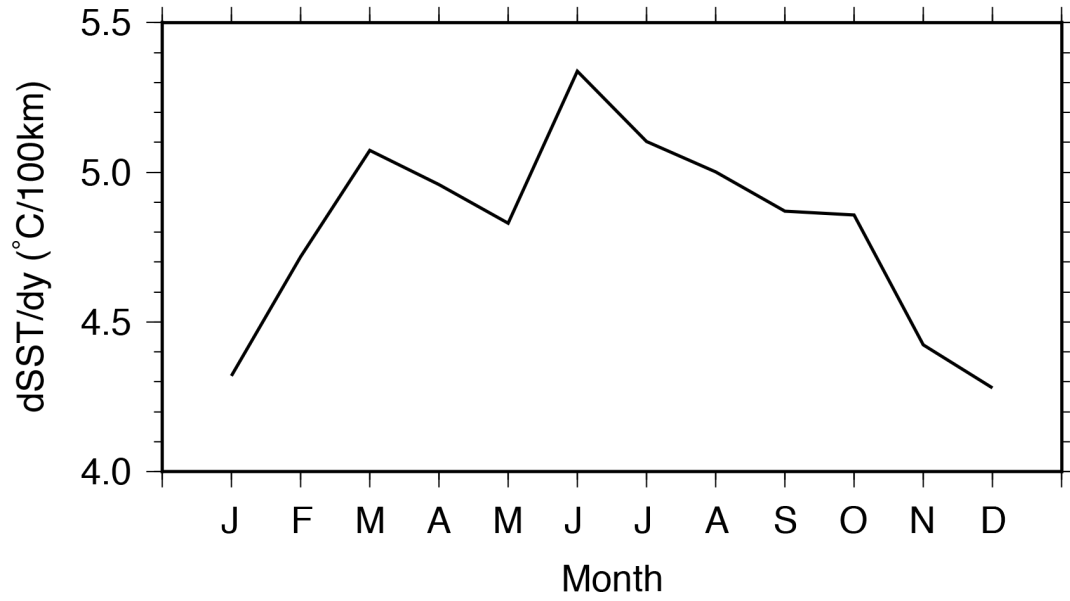


Fig. 2.4 Monthly climatology of the intensity of the SST front averaged over 40°–50°E.

With permission of Springer

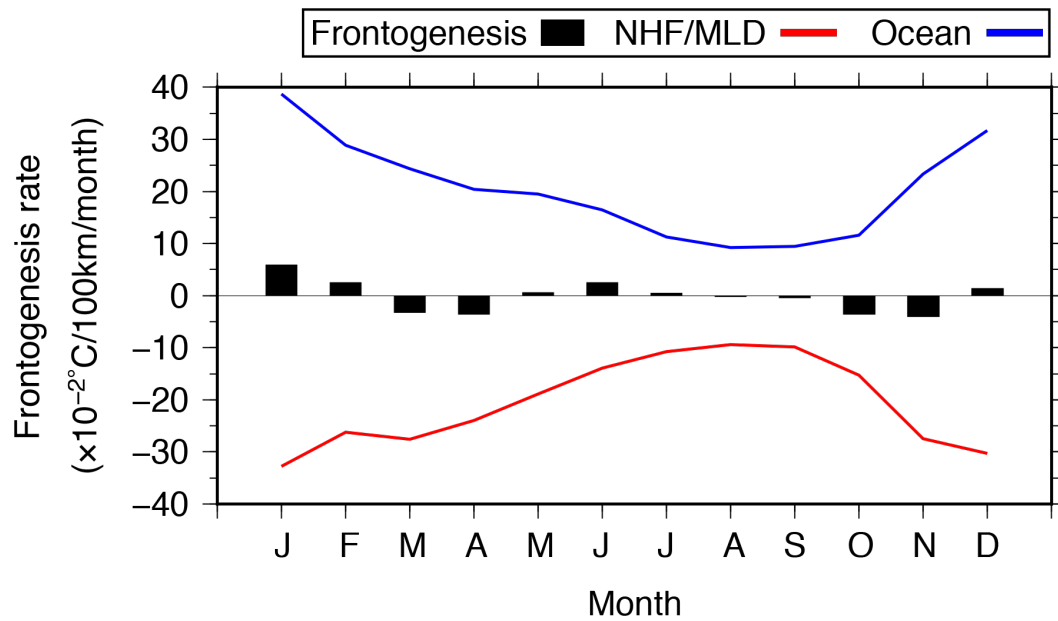


Fig. 2.5 Monthly climatology of the rate of frontogenesis [the left-hand side (LHS) term of Eq. (2.4); black bar], the NHF/MLD gradient term [the 1st term on the right-hand side (RHS) of Eq. (2.4); red line], and the meridional gradient of the oceanic term [the 2nd term on the RHS of Eq. (2.4); blue line]. With permission of Springer

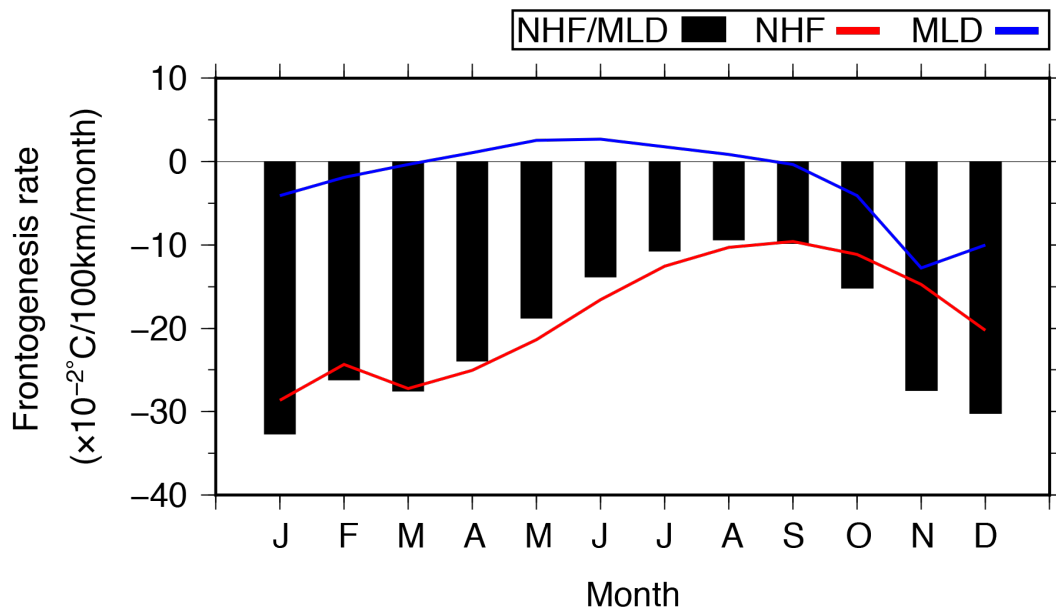


Fig. 2.6 Monthly climatology of each term in Eq. (2.5): the NHF/MLD gradient term (the LHS; black bar), the NHF gradient term (the 1st term on the RHS; red line), and the MLD gradient term (the 2nd term on the RHS; blue line). With permission of Springer

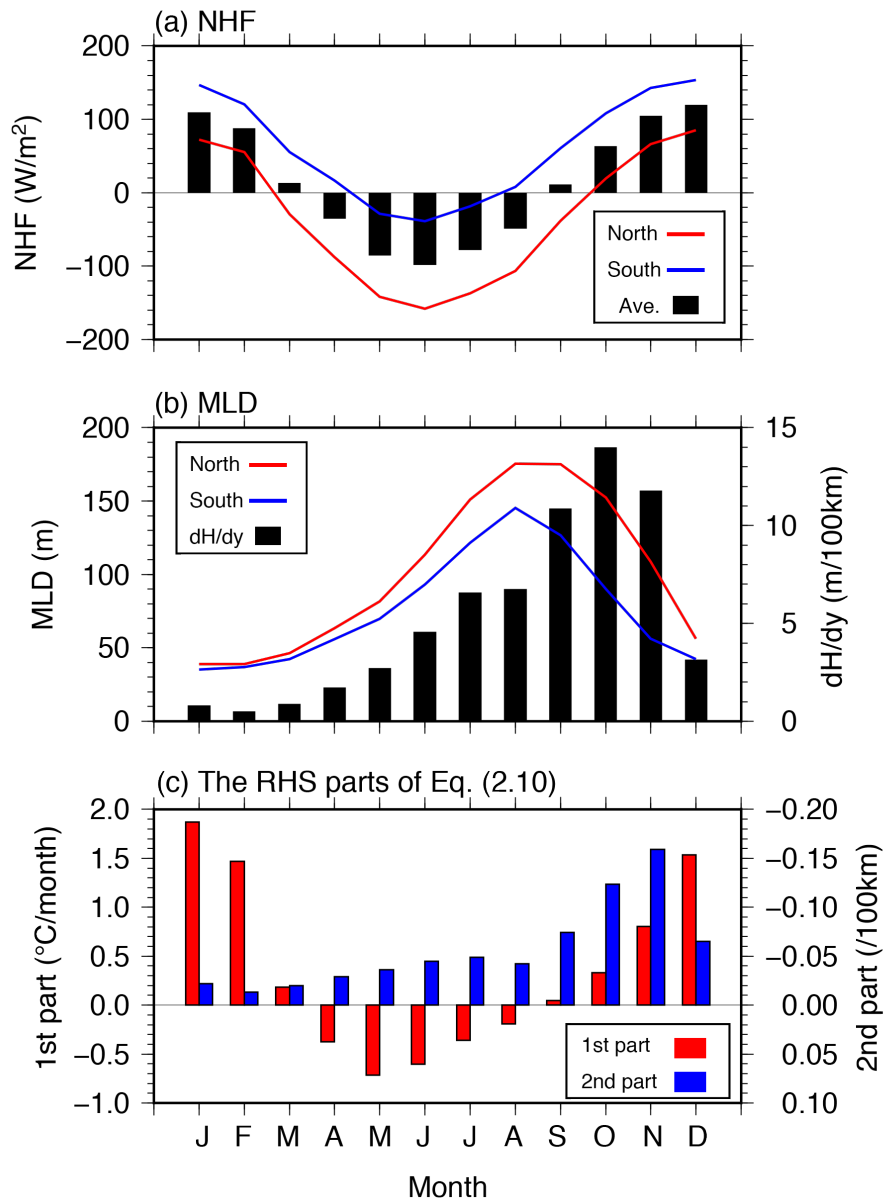


Fig. 2.7 Monthly climatology of the **a** NHF and **b** MLD in the northern (red line) and southern (blue line) regions. In **(a)**, the black bars indicate the NHF averaged within the northern and southern regions. In **(b)**, the black bars represent the MLD gradient. **c** Monthly climatology of the effect of heat flux on the mixed layer temperature (MLT) tendency [the 1st part on the RHS of Eq. (2.10); red bar] and the MLD gradient standardized by the MLD averaged within the northern and southern regions [the 2nd part on the RHS of Eq. (2.10); blue bar]. With permission of Springer

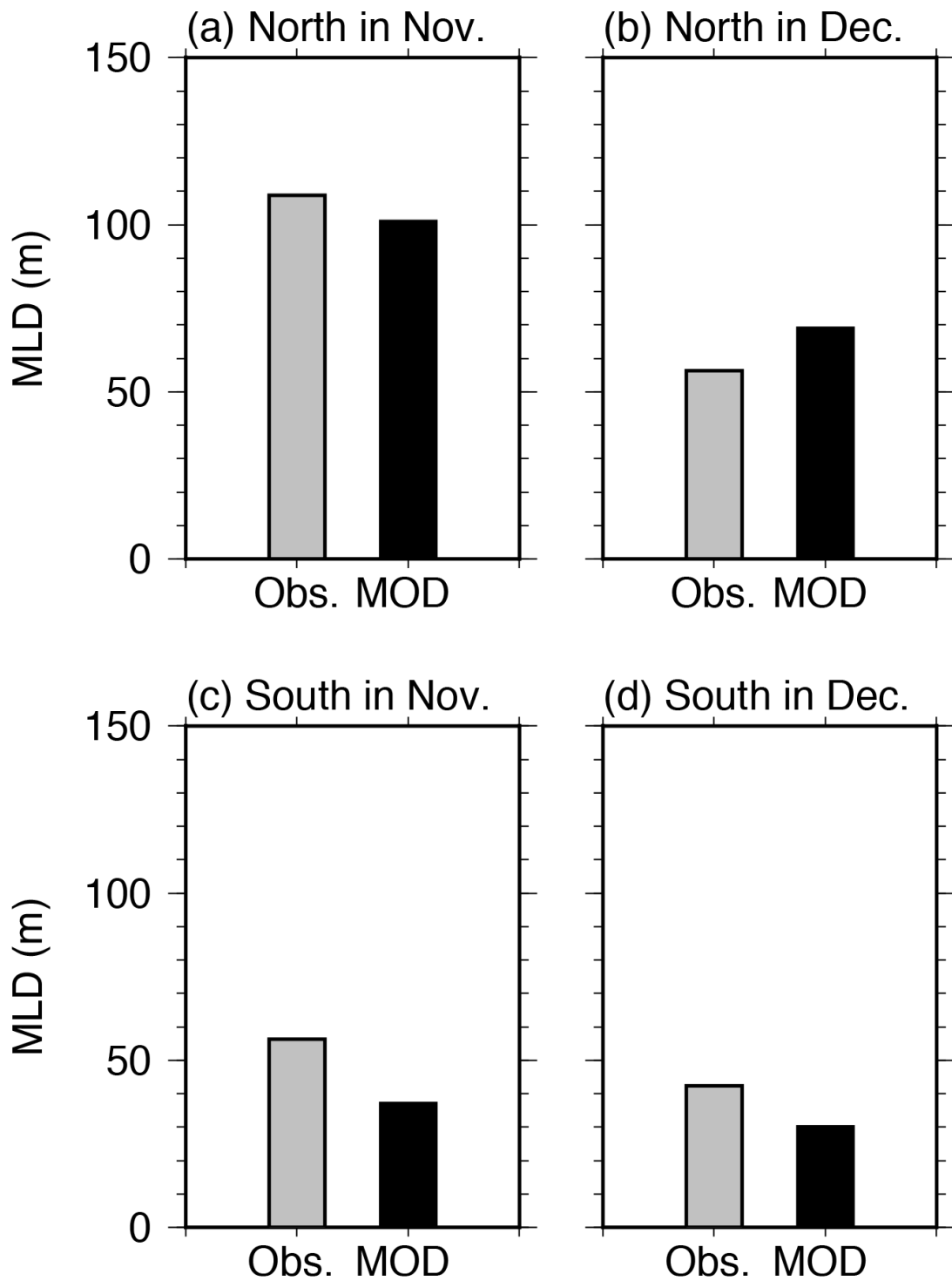


Fig. 2.8 Monthly climatology of the observed MLD (gray) and the Monin-Obukhov Depth (MOD; black) in the northern region in **a** November and **b** December. **c, d** As in **(a)** and **(b)**, but for the southern region. With permission of Springer

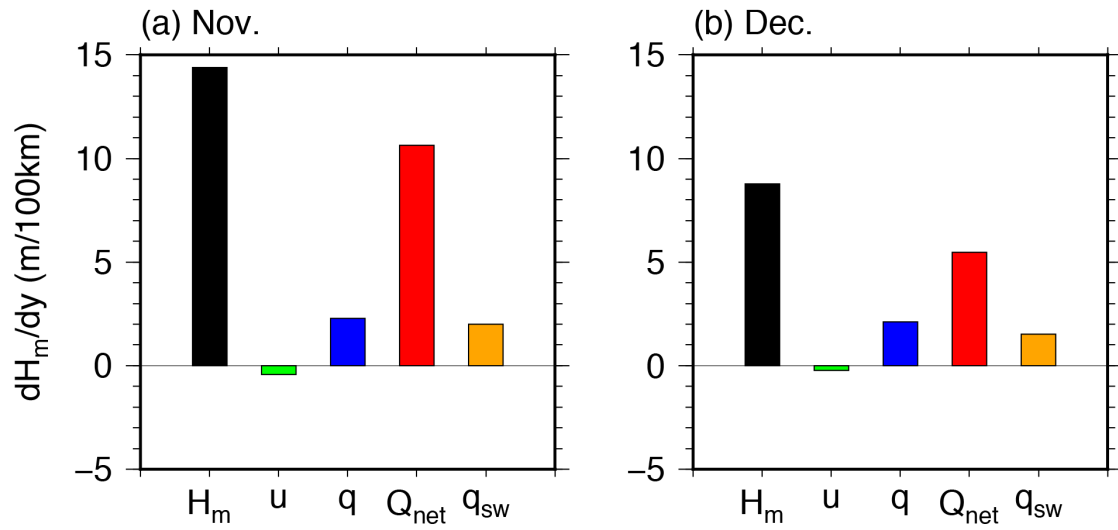


Fig. 2.9 Monthly climatology of each term in Eq. (2.6): the MOD gradient (the LHS; black) and the contribution from the gradient of wind speed (the 1st term on the RHS; green), incidence of shortwave radiation (the 2nd term on the RHS; blue), NHF (the 3rd term on the RHS; red), and downward shortwave radiation at the base of the MOD (the 4th term on the RHS; orange) in **a** November and **b** December. With permission of Springer

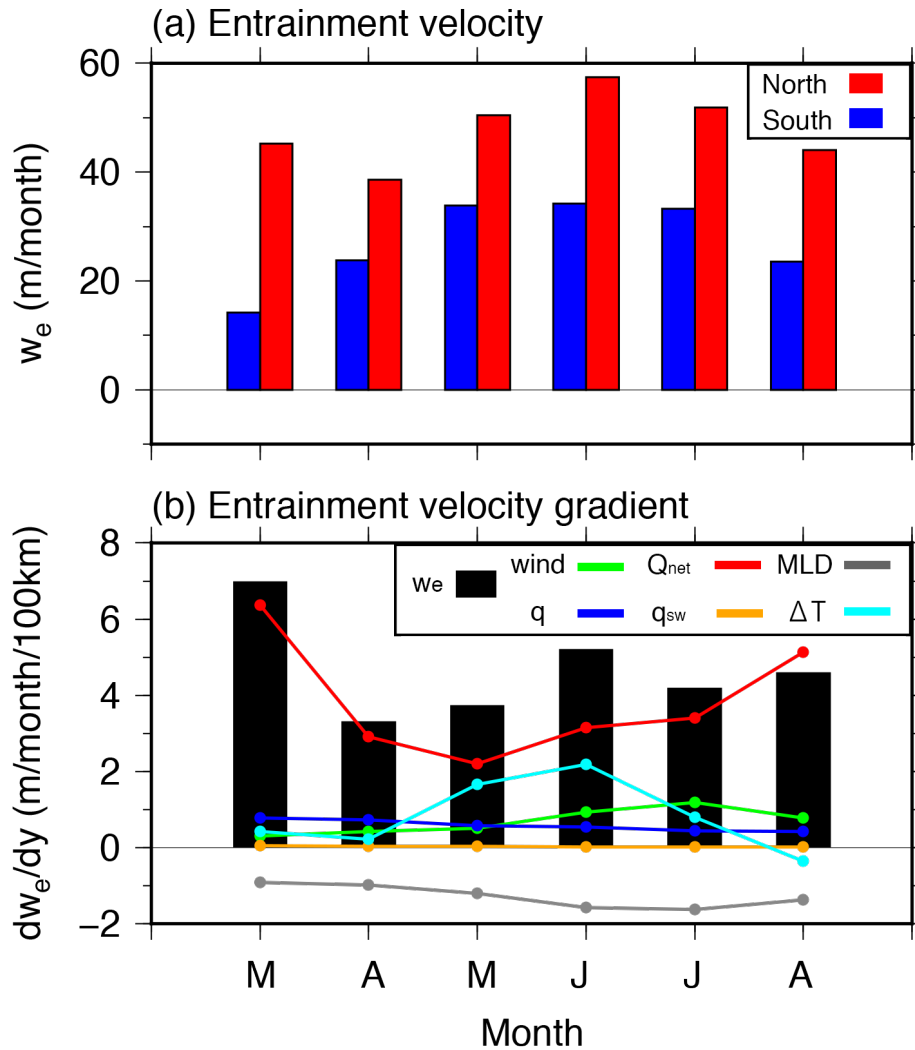


Fig. 2.10 Monthly climatology of **a** the diagnostic entrainment velocity in the northern (red) and southern (blue) regions, and **b** each term of Eq. (2.7) from March to August: the diagnostic entrainment velocity gradient (the LHS term; black bar) and the contribution from the gradient of wind speed (the 1st term on the RHS; green line), incidence of shortwave radiation (the 2nd term on the RHS; blue line), NHF (the 3rd term on the RHS; red line), downward shortwave radiation at the base of the mixed layer (the 4th term on the RHS; orange line), MLD (the 5th term on the RHS; gray line), and temperature difference (the 6st term on the RHS; cyan line). With permission of Springer

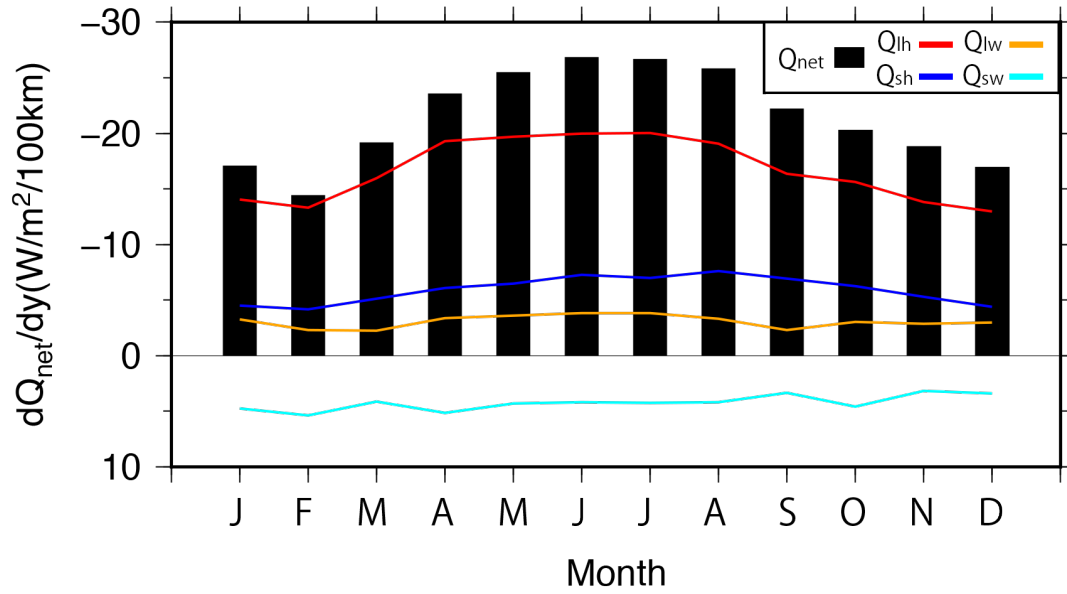


Fig. 2.11 Monthly climatology of each term in Eq. (2.8): the gradient of NHF (the LHS; black bar), latent heat flux (the 1st term on the RHS; red line), sensible heat flux (the 2nd term on the RHS; blue line), longwave radiation (the 3rd term on the RHS; orange line), and shortwave radiation (the 4th term on the RHS; cyan line). With permission of Springer

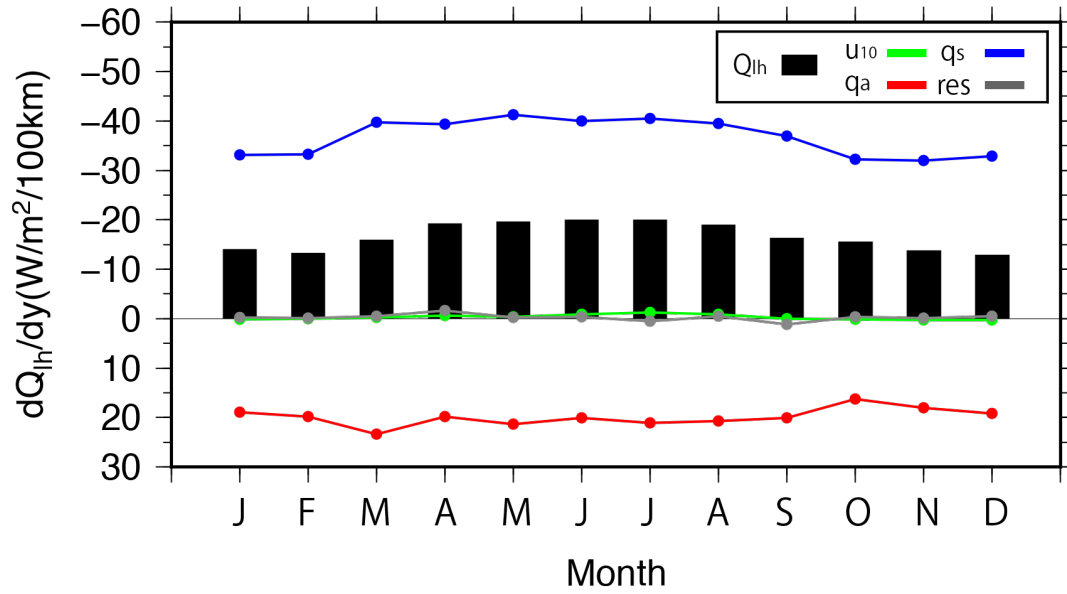


Fig. 2.12 Monthly climatology of each term in Eq. (2.9): the latent heat flux gradient (the LHS; black bar), the contribution from the gradient of wind speed (the 1st term on the RHS; green line), surface saturated specific humidity (the 2nd term on the RHS; blue line), and air specific humidity (the 3rd term on the RHS; red line), and the residual term (the 4th term on the RHS; gray line). With permission of Springer

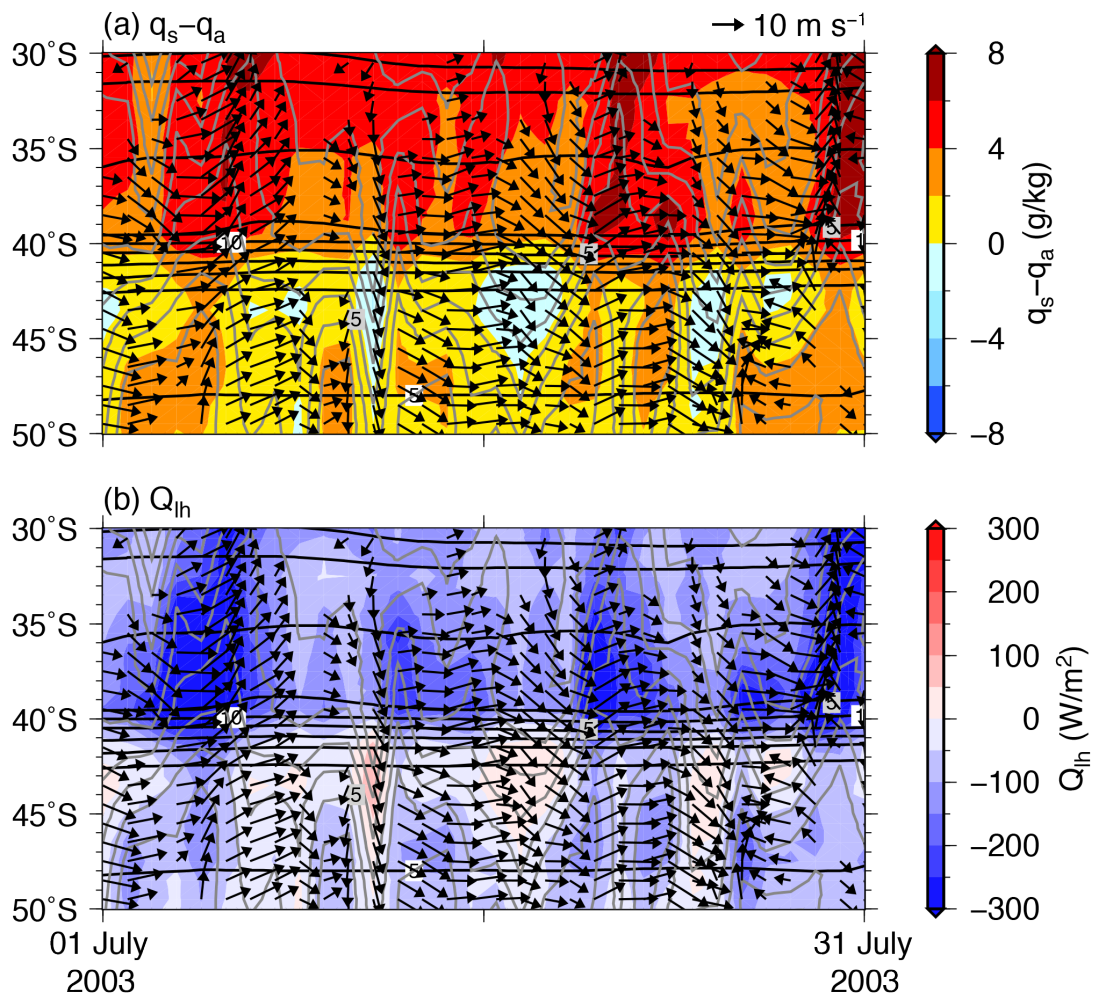


Fig. 2.13 Daily latitude-time sections of **a** the difference of the surface saturated and air specific humidity, and **b** the latent heat flux for 45.5°E in July 2003. Vectors represent surface wind greater than 5 m s⁻¹ and black (gray) contours indicate surface saturated (air) specific humidity. The vector scale is shown in the upper-right corner, and black and gray contour intervals are 1 g kg⁻¹

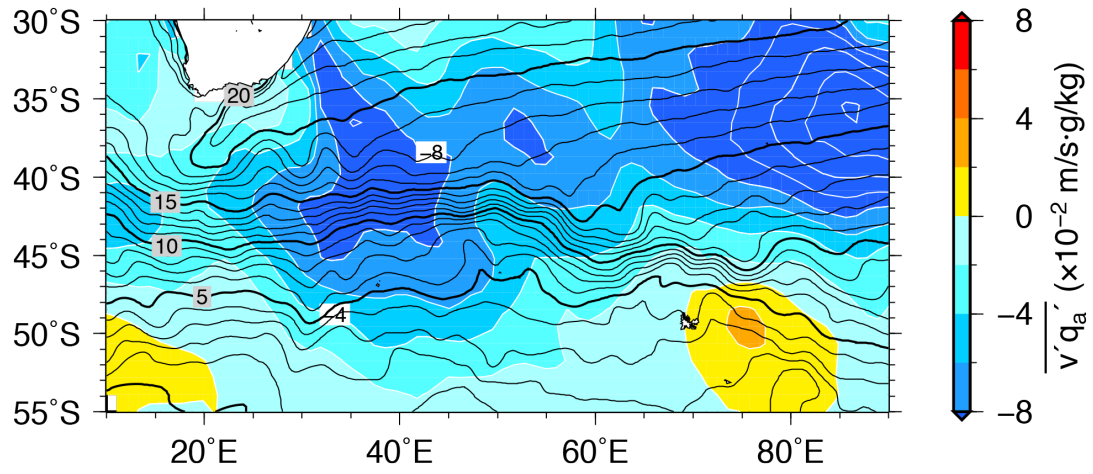


Fig. 2.14 Climatology of the meridional air specific humidity flux $\overline{v'q_a'}$ (color and white contour) and SST (black contour). White contour intervals are $2 \times 10^{-2} \text{ m s}^{-1} \text{ g kg}^{-1}$. Thin (Thick) black contour intervals are 1 (5) $^{\circ}\text{C}$

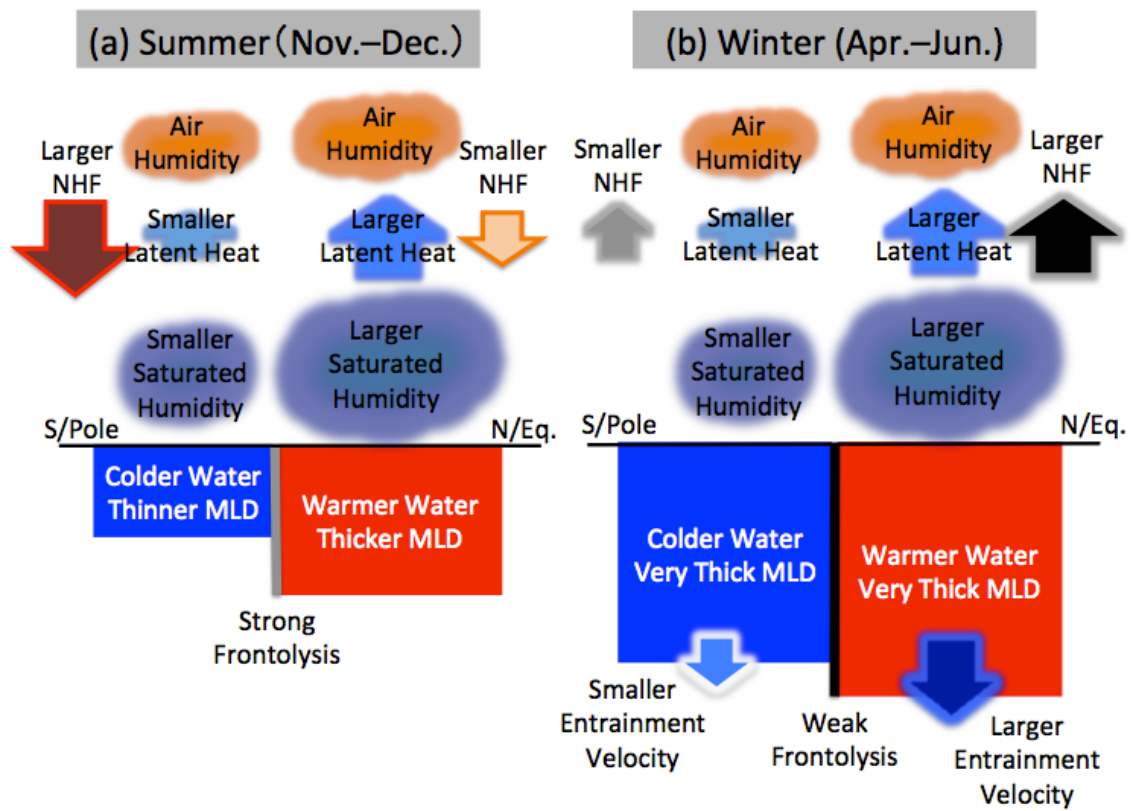


Fig. 2.15 Schematic diagrams of frontogenesis/frontolysis by the NHF and MLD gradient in austral **a** summer and **b** winter. With permission of Springer

Chapter 3

Frontogenesis in the Agulhas Return Current region simulated by a high-resolution CGCM

This chapter will be publicized within 5 years.

Chapter 4

General conclusions

4.1 Summary

In this thesis, frontogenesis and frontolysis of the sea surface temperature (SST) front in the Agulhas Return Current (ARC) region were investigated using observational datasets and a high-resolution couple general circulation model (CGCM). This section summarizes the main results obtained in each chapter (Fig. 4.1).

In Chapter 2, using observational datasets, the main features of the SST front in the ARC region were described, and the mechanisms of the frontogenesis/frontolysis were investigated quantitatively. In the ARC region, the strong SST front of $4\text{--}5\text{ }^{\circ}\text{C}\ 100\text{km}^{-1}$ is found in $20^{\circ}\text{--}70^{\circ}\text{E}$. It is located within $45^{\circ}\text{--}40^{\circ}\text{S}$ and its location is relatively stable especially in $40^{\circ}\text{--}70^{\circ}\text{E}$. Also, there is seasonality with slightly weaker (stronger) intensity in austral summer (winter). Due to rough balance between frontolysis by the surface net heat flux (NHF) and frontogenesis by oceanic processes, the intensity of the SST front is maintained throughout the year. Since the number of velocity observations in the ocean interior is insufficient, oceanic processes are estimated as residual. Therefore, only detailed mechanisms of frontolysis by the NHF were examined.

The SST front induces large meridional difference with higher (lower) surface saturated humidity on the northern (southern) region, while meridional difference in air specific humidity is small due to meridional humidity advection with the passage of atmospheric disturbances. Therefore, the SST front causes larger (smaller) latent heat release on the northern (southern) side through the formation of larger (smaller) air-sea specific humidity difference.

In austral summer, shortwave radiation strongly heats the sea surface, but it is partially offset by the larger (smaller) latent heat release north (south) of the front. Thus,

the surface warming is weaker (stronger) north (south) of the front, and the NHF relaxes the SST front. At the same time, the weaker warming on the northern side leads to deeper mixed layer compared to the southern side. Since the thicker (thinner) mixed layer in the northern (southern) region is less (more) sensitive to surface warming, the mixed layer depth (MLD) gradient strengthens the frontolysis. In addition, seasonally thin mixed layer amplifies the frontolysis.

On the other hand, stronger (weaker) surface cooling due to the larger (smaller) latent heat release north (south) of the front leads to frontolysis in austral winter. However, the frontolysis is weakened, because the stronger (weaker) cooling on the northern (southern) side induces larger (smaller) entrainment velocity, and the resulting thicker (thinner) mixed layer is less (more) sensitive to surface cooling. In addition, the seasonally thick mixed layer further weakens the frontolysis. Therefore, the NHF strongly (weakly) relaxes the SST front through mixed layer processes in austral summer (winter).

In Chapter 3, frontogenesis by oceanic processes in the ARC region, which was estimated as residual in Chapter 2, was investigated quantitatively using a high-resolution CGCM, the Community Earth System Model (CESM; Hurrell et al. 2013; Small et al. 2014). The CESM realistically simulates the main characteristics of the SST front and MLD in the ARC region. Also, the simulated frontolysis by the NHF and frontogenesis by oceanic processes are in good agreement with the observation. Among the oceanic processes, the contribution from the horizontal advection is most dominant, while the entrainment has a minor contribution.

Frontogenesis by the horizontal advection is caused by cross-isotherm confluence with warmer (cooler) temperature advection toward the SST front on the

northern (southern) side, and this structure is seen from the sea surface to about 1000 m depth. The importance of the advection by weak meridional confluent flow rather than that by strong zonal along-isotherm flow in reinforcing the SST front in the ARC region is an intriguing result. Due to the stronger (smaller) cross-isotherm confluence, which may be related to the strength of the Agulhas Current, ARC, and ACC, the frontogenesis by the horizontal advection is stronger (weaker) in austral summer (winter).

To gain dynamical insight into the confluent flow, vorticity balance in the frontal region was examined. Due to meridional asymmetry in the relative vorticity in the analysis region, the strong eastward time-mean along-isotherm current advects smaller cyclonic (larger anticyclonic) vorticity north (south) of the front. On the other hand, southward and northward velocity perturbations associated with meanderings are formed over anticyclonic and cyclonic relative vorticity perturbations, respectively. Both velocity perturbations advect cyclonic (anticyclonic) vorticity on the northern (southern) side. These meridional differences of the cyclonic (anticyclonic) eddy cross-isotherm and mean along-isotherm vorticity advection on the northern (southern) side are in balance with the anticyclonic (cyclonic) vorticity advection by the mean cross-isotherm confluence.

In contrast to the NHF and horizontal advection, the entrainment does not contribute much to frontogenesis/frontolysis. This is because three factors related to the frontogenesis/frontolysis by the entrainment cancel each other out. As described above, the stronger surface cooling in the northern region induces the larger entrainment velocity, and thus the deeper mixed layer is formed compared to the southern region. Due to the larger (smaller) entrainment velocity on the northern (southern) side, the

mixed layer entrains larger (smaller) amount of cold water from the lower layer. Thus, the entrainment velocity gradient contributes to frontolysis. In contrast, the MLD gradient acts as frontogenesis, because the thicker (thinner) mixed layer in the northern (southern) region is less (more) sensitive to cooling by the entrainment. Also, the meridional gradient in the temperature difference between the mixed layer and entrained water results in frontogenesis. This is because the mixed layer entrains less (more) cold water from the lower layer owing to the smaller (larger) temperature difference north (south) of the front. The weak stratification in the northern region may be associated with the Mode Water formation processes (e.g. Hanawa and Talley 2001; Tsubouchi et al. 2010; Oka and Qiu 2012) that vertically uniform structure is formed due to the wintertime deep mixed layer.

In summary, the SST front in the ARC region is maintained throughout the year due to the approximate balance between the frontogenesis by the horizontal advection associated with the cross-isotherm confluence and the frontolysis by the NHF modified through mixed layer processes. This study is the first to quantitatively investigate the mechanisms of frontogenesis/frontolysis in mid-latitude SST fronts. In this thesis, we have revealed important roles of the MLD for the frontolysis by the NHF and the cross-isotherm confluence for the frontogenesis by the horizontal advection.

4.2 Concluding remarks

Vorticity balance in the ARC region discussed in Chapter 3 suggests the importance of the eddy-mean interaction for the cross-isotherm confluence, but the causes of the cross-isotherm confluence are not yet completely revealed. This is partly because the SST front was already established in the CGCM. In this regard, idealized

models as in previous studies (e.g. Samelson 1993; Thompson 2000; Waterman and Jayne 2011) may be useful, but they cannot to incorporate realistic factors such as the atmospheric forcing and ocean interior structure. For this reason, it may be a good idea to try an “idealized” coupled model experiment, in which a coupled model with a rectangular domain and flat bottom is integrated from an initial condition with a horizontal uniform temperature/salinity field forced by meridionally varying shortwave radiation at the top of the atmosphere. It is expected that western boundary currents and SST fronts are generated in the mid-latitudes associated with the wind-driven circulation. Analyzing this spin-up stage in detail by examining frontogenesis/frontolysis, vorticity balance, and energetics may provide useful insight. Furthermore, conducting sensitivity experiments with the same coupled model can further disentangle importance of various processes related to frontogenesis/frontolysis. For instance, sensitivity to MLD can be examined by changing the vertical mixing coefficient, and sensitivity to strength of western boundary currents may be checked by modifying atmospheric circulation through changes in meridional gradient of shortwave radiation. Also, since an influence of bottom topography on the SST front in the ARC region is hinted, the coupled model can be used to investigate a role of topography in frontogenesis/frontolysis of SST fronts. The above is a topic for future research.

As described in Chapter 1, recent studies (Morioka et al. 2015; Ohishi et al. 2015) pointed out interannual variations of the SST front in the ARC region may modulate the Mascarene High, which plays a key role in development of an interannual climate mode called the Indian Ocean Subtropical Dipole (IOSD; e.g. Behera and Yamagata 2001), through their influence on storm track activity. However, there was a lack of fundamental understanding regarding frontogenesis/frontolysis processes in the

ARC region. The present study, thus, contributes to better understanding of interannual variations in the South Indian Ocean. Also, this study infers possible existence of a positive feedback process of the IOSD that has never been discussed. During a positive IOSD event, changes in the Mascarene High results in advection of more moist air from the tropics to the southwestern pole of the IOSD (Chiodi and Harrison 2007; Morioka et al. 2012), which is located to the north of the SST front in the ARC region. As a result, mixed layer becomes anomalously shallow owing to reduced latent heat release and positive SST anomalies are generated owing to more efficient warming of the mixed layer by climatological shortwave radiation (Morioka et al. 2010; Morioka et al. 2012). Consequently, this may amplify the positive IOSD event by affecting the Mascarene High, because a stronger SST front may enhance the feedback from the storm track activity to the subtropical high as suggested by Miyasaka and Nakamura (2010). Coupled model experiments initiating from an anomalously strong/weak oceanic front in the ARC region may help us to further clarify the interaction among the SST front, storm track activity, Mascarene High, and SST anomalies associated with the IOSD.

The analysis methods of this study can be applied to other SST fronts in mid-latitudes such as those in the Kuroshio Extension, Gulf Stream (e.g. Kelly et al. 2010; Kwon et al. 2010), and Brazil–Malvinas Confluence region (e.g. Saraceno et al. 2004; Tokinaga et al. 2005). Each of the above SST fronts has its unique character in horizontal distribution, seasonality, overlying atmosphere, and ocean interior field. For instance, a single sharp SST front is found in the Gulf Stream region as in the ARC region, while a number of fronts, such as subtropical and subpolar fronts, are distributed in the Kuroshio Extension and Brazil–Malvinas Confluence regions.

As an extension of this study, Tozuka et al. (manuscript submitted to

Scientific Reports) examined the wintertime strengthening of the SST front in the Kuroshio Extension region. Remarkably, they found that the NHF term acts as frontogenesis. This results from the relatively small meridional gradient in the NHF associated with the winter monsoon effects (Konda et al. 2010) and the large MLD gradient in the frontal region. When the northerly winds from the continent are prominent, meridional difference of latent heat release is small, because the contribution from stronger (weaker) wind speed north (south) of the front compensates for that from smaller (larger) air-sea specific humidity difference. On the other hand, larger (smaller) air-sea temperature difference and stronger (weaker) wind speed induces larger (smaller) sensible heat release on the northern (southern) side. As a result, turbulent heat release is larger (smaller) in the northern (southern) region during northerly wind events. In contrast, the turbulent heat release is smaller (larger) north (south) of the front during other time. This is because the meridional gradient in sensible heat release is relatively small, while latent heat release is smaller (larger) on the northern (southern) side due to larger (smaller) air-sea specific humidity difference. Consequently, the meridional difference of turbulent heat release is small for wintertime mean, and the small NHF gradient does not contribute much to frontogenesis/frontolysis in the Kuroshio Extension region. On the other hand, the large MLD gradient with a shallower (deeper) mixed layer on the northern (southern) side exists owing to shallower (deeper) thermocline. Since the thinner (thicker) mixed layer north (south) of the front is more (less) sensitive to surface cooling, the MLD gradient favors frontogenesis.

Although the focus of this study is on the seasonal timescale, SST fronts in mid-latitudes are known to undergo interannual-to-decadal variations. In the Kuroshio Extension region, for example, decadal variations in the SST front are detected (e.g. Qiu

and Chen 2005) and have substantial influences on the atmosphere (Masunaga et al. 2016). Also, decadal variations in the MLD south of the front are generated due to combined effects of westward Rossby wave forced by wind stress curl in the central North Pacific and mesoscale eddy activity associated with changes in the flow path state (Qiu and Chen 2006; Sugimoto and Kako 2016). It will be interesting to quantitatively investigate the causes of decadal variations in frontogenesis/frontolysis in the Kuroshio Extension region by applying the present method with a special focus on meridional gradient in the MLD.

Also, we note that SST fronts are not limited to the mid-latitudes. In the eastern tropical Pacific and Atlantic regions, sharp SST fronts accompanying tropical instability waves (TIWs) are observed north of the cold tongues (e.g. Düing et al. 1975; Legeckis 1977; Jochum et al. 2004; Willett et al. 2006). These cold tongues and TIWs persist from July to November when the strong easterly trade winds induce equatorial upwelling. Particularly in the tropical Pacific, they undergo interannual variations; they are weaker (stronger) during El Niño (La Niña) (Contreras 2002; Yu and Liu 2003). Since buoy observations by Tropical Atmosphere Ocean (TAO)/TRIangle Trans-Ocean buoy Network (TRITON) array in the tropical Pacific (McPhaden 1995; Ando and Kuroda 2002) and Prediction and Research Moored Array in the Atlantic (PIRATA) array in the tropical Atlantic (Bourlès et al. 2008) are maintained for decades, we may quantitatively investigate frontogenesis/frontolysis in the tropical oceans on seasonal-to-interannual time scales using observational data. Since the SST fronts accompanying the TIWs also have substantial influences on the atmosphere (e.g. Xie et al. 1998; Hashizume et al. 2001), the method proposed by the present study may shed new light on the tropical air-sea interaction.

This study benefitted from the recent progress in observational network by the Argo floats, which enabled us to capture frontal-scale structure in the ocean interior and allowed us to conduct the mixed layer temperature (MLT) balance analysis. Without sufficient data in the ocean interior provided by the Argo floats, the sharp MLD gradient in the ARC region may have been smeared out by a large radius of influence needed to prepare a gridded dataset, and the frontolysis by the NHF could not be estimated accurately. Therefore, it is strongly recommended to maintain and even enhance the global coverage by the Argo floats.

The results presented in Chapter 3 are from a single CGCM. It will be interesting to analyze outputs from the High Resolution Model Intercomparison Project (HighResMIP; Haarsma et al. 2016), one of the Coupled Model Intercomparison Project Phase 6 (CMIP6; Eyring et al. 2016) Endorsed Model Intercomparison Projects. This study has suggested that it is crucial to simulate horizontal distribution of the MLD to realistically simulate SST fronts in mid-latitudes. Excessively deep mixed layer, for example, may cause SST fronts to become erroneously strong, because such a bias weakens frontolysis owing to less sensitivity to the NHF. Since it is demonstrated that SST fronts impact on storm track activity in mid-latitudes (e.g. Nakamura et al. 2008; Ogawa et al. 2012), the above bias impairs not only local atmospheric fields, but also global scale atmospheric fields. Thus, further improvements in mixed layer parameterizations in the ocean component (Furuichi et al. 2012; Watanabe and Hibiya 2013) are of crucial importance for more realistic simulations by CGCMs.

Figure

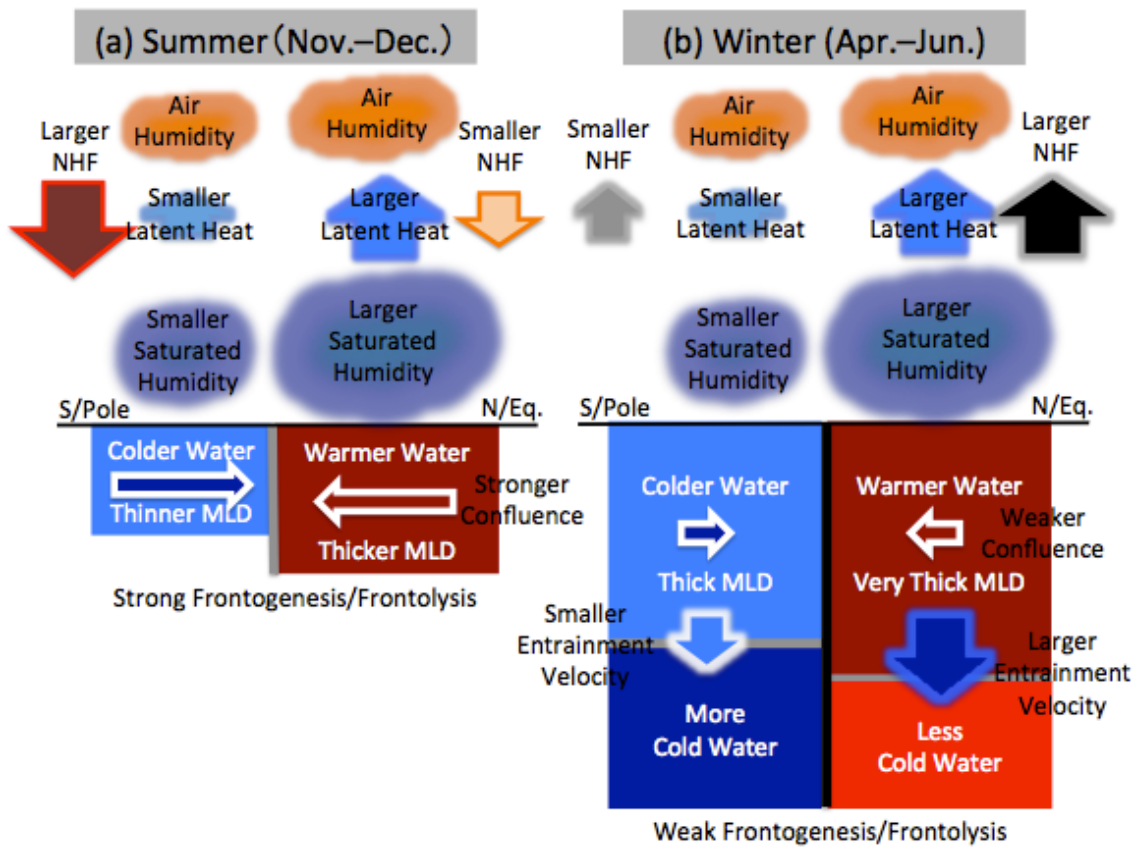


Fig. 4.1 Schematic diagrams of frontogenesis/frontolysis by the NHF, horizontal advection, entrainment in austral **a** summer and **b** winter

Acknowledgments

I would like to express my sincere gratitude to my supervisor, Tomoki Tozuka, for his continuous support and ceaseless encouragement. His courteous guidance promoted my research and allowed me to develop as a research scientist. I am also indebted to him for taking his time to check my thesis in spite of a birth of his son.

I would like to thank my dissertation committee members, Ichiro Yasuda, Toshiyuki Hibiya, Yukio Masumoto, and Hisashi Nakamura for their time and helpful comments. I am deeply grateful to Meghan F. Cronin for her warm support and guidance of my research during my internship at NOAA Pacific Marine Environmental Laboratory. She provided insightful advice that broadened my horizons and gave me opportunities to interact with researchers at her institutions. This study benefitted from discussions with Nobumasa Komori, Masami Nonaka, Takeshi Doi, and Yushi Morioka in JAMSTEC, Hiroaki Miura, Kunihiro Aoki, Bunmei Taguchi, Yu Kosaka, and Takafumi Miyasaka in the University of Tokyo, Kimio Hanawa, Toshio Suga, Shoichi Kizu, and Shusaku Sugimoto in Tohoku University, and Kazuaki Nishii in Mie University.

I am also thankful to Yoshihiro Niwa, Chie Ihara, Yuki Tanaka, Takaaki Yokoi, Taira Nagai, Masashi Kohma, Takahito Kataoka, Takashi Ijichi, Shota Katsura,

Yuki Yasuda, Yoko Yamagami, Tamaki Suematsu, Tsubasa Kohyama, Masatoshi Miyamoto, Ayumu Miyamoto, Arata Amemiya, Hajime Ishii, Chiarui Ong, Satoru Endo, Chiho Tanizaki, Ryosuke Yasui, Shoichiro Kido, Anne Takahashi, Katsutoshi Fukuzawa, Shuhei Matsugishi, Wei Yang, Emiri Kobori, Marvin Seow, Daiki Ito, Ryohei Yamaguchi, and all past and present members of Atmospheric and Oceanic Science Group in the University of Tokyo and Physical/Satellite Oceanography Laboratory in Tohoku University for their valuable discussion, encouragement, and help. Besides, I owe deep gratitude to my classmates, Yohei Onuki, Hidetaka Kobayashi, Sam Sherriff-Tadano, Takashi Obase, Tomoaki Takagi, Ryosuke Shibuya, Yuya Ozawa, Satoru Okajima, Ryusuke Masunaga, Kenta Sueki, Kota Hirabayashi, Takafumi Kaneko, Tatsuhiro Mori, Lisa Ito, Yasuharu Seo, Yu Shibata, Kaori Hikobe, Ryosuke Sasaki, Shinichi Murase, Masanori Saito, Takashi Matsuda, and Tsukasa Tekuramori. Thanks to them, I was able to have an enjoyable life in the University of Tokyo and Tohoku University. I also appreciate warm cordial reception from members of NOAA Pacific Marine Environmental Laboratory and University of Washington during my internship.

I would like to acknowledge financial support from the Japan Society for Promotion of Science through Grant-in-Aid for Scientific Research on Innovative Areas 2205, The Japan Science Society from the Sasakawa Scientific Research Grant, Iwadare Scholarship Foundation, The Oceanographic Society of Japan for overseas travel expenses, and the University of Tokyo Ocean Alliance for overseas internship.

Finally, I would like to express my deepest appreciation to my mother, my sister, my dog, and my grandparents. I feel most grateful for their support to my decision to go on to the doctoral program. This thesis could not have been completed without their warm support and encouragement.

References

- Akima H (1970) A new method of interpolation and smooth curve fitting based on local procedures. *J Assoc Comput Mach* 17:589–602. doi: 10.1145/321607.321609
- Ando K, Kuroda Y (2002) Two modes of salinity and temperature variation in the surface layer of the Pacific Warm Pool. *J Oceanogr* 58:599–609. doi: 10.1023/A:1021223028579
- Beal LM, de Ruijter WPM, Biastoch A, Zahn R (2011) On the role of the Agulhas system in ocean circulation and climate. *Nature* 472:429–436. doi: 10.1038/nature09983
- Behera SK, Yamagata T (2001) Subtropical SST dipole events in the southern Indian Ocean. *Geophys Res Lett* 28:327–330. doi: 10.1029/2000GL011451
- Boebel O, Rossby T, Lutjeharms J, Zenk W, Barron C (2003) Path and variability of the Agulhas Return Current. *Deep Sea Res Part II* 50:35–56. doi: 10.1016/S0967-0645(02)00377-6
- Bourlès B, Lumpkin R, McPhaden MJ, Hernandez F, Nobre P, Campos E, Yu L, Planton S, Busalacchi A, Moura AD, Servain J, Trotte J (2008) The PIRATA Program: History, accomplishments, and future directions. *Bull Am Meteorol Soc* 89:1111–1125. doi: 10.1175/2008BAMS2462.1

- Cayan DR (1992) Latent and sensible heat flux anomalies over the Northern Oceans: Driving the sea surface temperature. *J Phys Oceanogr* 22:859–881. doi: 10.1175/1520-0485(1992)022<0859:LASHFA>2.0.CO;2
- Chelton DB, Schlax MG, Freilich MH, Milliff RF (2004) Satellite measurements reveal persistent small-scale features in ocean winds. *Science* 303:978–983. doi: 10.1126/science.1091901
- Chelton DB, Schlax MG, Witter DL, Richman JG (1990) Geosat altimeter observations of the surface circulation of the Southern Ocean. *J Geophys Res* 95:17877–17903. doi: 10.1029/JC095iC10p17877
- Chelton DB, Wentz FJ (2005) Global microwave satellite observations of sea surface temperature for numerical weather prediction and climate research. *Bull Am Meteorol Soc* 86:1097–1115. doi: 10.1175/BAMS-86-8-1097
- Chiodi AM, Harrison DE (2007) Mechanisms of summertime subtropical southern Indian Ocean sea surface temperature variability: On the importance of humidity anomalies and the meridional advection of water vapor. *J Clim* 20:4835–4852. doi: 10.1175/JCLI4271.1
- Contreras RF (2002) Long-term observations of tropical instability waves. *J Phys Oceanogr* 32:2715–2722. doi: 10.1175/1520-0485-32.9.2715
- Cronin M (1996) Eddy-mean flow interaction in the Gulf Stream at 68°W. Part II: Eddy forcing on the time-mean flow. *J Phys Oceanogr* 26:2132–2151. doi: 10.1175/1520-0485(1996)026<2132:EMFIIT>2.0.CO;2
- Cronin MF, Tozuka T (2016) Steady state ocean response to wind forcing in extratropical frontal regions. *Sci Rep* 6:28842. doi: 10.1038/srep28842
- Davis RE, DeSzoeko R, Niiler P (1981) Variability in the upper ocean during MILE.

- Part II: Modeling the mixed layer response. *Deep Sea Res* 28:1453–1475. doi: 10.1016/0198-0149(81)90092-3
- De Boer AM, Graham RM, Thomas MD, Kohfeld KE (2013) The control of the Southern Hemisphere westerlies on the position of the subtropical front. *J Geophys Res Ocean* 118:5669–5675. doi: 10.1002/jgrc.20407
- Deardorff JW, Willis GE, Lilly DK (1969) Laboratory investigation of non-steady penetrative convection. *J Fluid Mech* 35:7–31. doi: 10.1017/S0022112069000942
- Dee DP, Uppala SM, Simmons AJ, Berrisford P, Poli P, Kobayashi S, Andrae U, Balmaseda MA, Balsamo G, Bauer P, Bechtold P, Beljaars ACM, van de Berg L, Bidlot J, Bormann N, Delsol C, Dragani R, Fuentes M, Geer AJ, Haimberger L, Healy SB, Hersbach H, Hólm EV, Isaksen L, Kållberg P, Köhler M, Matricardi M, McNally AP, Monge-Sanz BM, Morcrette JJ, Park BK, Peubey C, de Rosnay P, Tavolato C, Thépaut JN, Vitart F (2011) The ERA-Interim reanalysis: Configuration and performance of the data assimilation system. *Quart J Roy Meteor Soc* 137:553–597. doi: 10.1002/qj.828
- Delman AS, McClean JL, Sprintall J, Talley LD, Yulaeva E, Jayne SR (2015) Effects of eddy vorticity forcing on the mean state of the Kuroshio Extension. *J Phys Oceanogr* 45:1356–1375. doi: 10.1175/JPO-D-13-0259.1
- Ducet N, Le Traon PY, Reverdin G (2000) Global high-resolution mapping of ocean circulation from TOPEX/Poseidon and ERS-1 and -2. *J Geophys Res* 105:19477–19498. doi: 10.1029/2000JC900063
- Düing W, Hisard P, Katz E, Meincke J, Miller L, Moroshkin KV, Philander G, Ribnikov AA, Voigt K, Weisberg R (1975) Meanders and long waves in the equatorial Atlantic. *Nature* 257:280–284. doi:10.1038/257280a0

- Eyring V, Bony S, Meehl GA, Senior CA, Stevens B, Stouffer RJ, Taylor KE (2016) Overview of the Coupled model intercomparison project phase 6 (CMIP6) experimental design and organization. *Geosci Model Dev* 9:1937–1958. doi: 10.5194/gmd-9-1937-2016
- Fairall CW, Bradley EF, Hare JE, Grachev AA, Edson JB (2003) Bulk parameterization of air-sea fluxes: Updates and verification for the COARE algorithm. *J Clim* 16:571–591. doi: 10.1175/1520-0442(2003)016<0571:BPOASF>2.0.CO;2
- Fauchereau N, Trzaska S, Richard Y, Roucou P, Camberlin P (2003) Sea-surface temperature co-variability in the southern Atlantic and Indian Oceans and its connections with the atmospheric circulation in the Southern Hemisphere. *Int J Climatol* 23:663–677. doi: 10.1002/joc.905
- Feliks Y, Ghil M, Simonnet E (2004) Low-frequency variability in the midlatitude baroclinic atmosphere induced by an oceanic thermal front. *J Atmos Sci* 61:961–981. doi: 10.1175/JAS3780.1
- Frankignoul C (1985) Sea surface temperature anomalies, planetary waves, and air-sea feedback in the middle latitudes. *Rev Geophys* 23:357–390. doi: 10.1029/RG023i004p00357
- Furuichi N, Hibiya T, Niwa Y (2012) Assessment of turbulence closure models for resonant inertial response in the oceanic mixed layer using a large eddy simulation model. *J Oceanogr* 68:285–294. doi: 10.1007/s10872-011-0095-3
- Haarsma RJ, Roberts MJ, Vidale PL, Senior CA, Bellucci A, Bao Q, Chang P, Corti S, Fučkar NS, Guemas V, von Hardenberg J, Hazeleger W, Kodama C, Koenigk T, Leung LR, Lu J, Luo J-J, Mao J, Mizielinski MS, Mizuta R, Nobre P, Satoh M, Scoccimarro E, Semmler T, Small J, von Storch J-S (2016) High resolution model

- intercomparison project (HighResMIP v1.0) for CMIP6. *Geosci Model Dev* 9:4185–4208. doi: 10.5194/gmd-9-4185-2016
- Hanawa K, Talley LD (2001) Mode Waters. In: Siedler G, Griffies SM, Gould J, Church JA (eds) *Ocean circulation and climate*. Academic Press, Cambridge, pp 373–386
- Hashizume H, Xie S-P, Liu WT, Takeuchi K (2001) Local and remote atmospheric response to tropical instability waves: A global view from space. *J Geophys Res* 106:10173–10185. doi: 10.1029/2000JD900684
- Hermes JC, Reason CJC (2005) Ocean model diagnosis of interannual coevolving SST variability in the South Indian and South Atlantic Oceans. *J Clim* 18:2864–2882. doi: 10.1175/JCLI3422.1
- Hoskins BJ (1971) Atmospheric frontogenesis models: Some solutions. *Quart J Roy Meteor Soc* 97: 139–153. doi: 10.1002/qj.49709741202
- Hoskins BJ, Bretherton FP (1972) Atmospheric frontogenesis models: Mathematical formulation and solution. *J Atmos Sci* 29:11–37. doi: 10.1175/1520-0469(1972)029<0011:AFMMFA>2.0.CO;2
- Hunke EC, Lipscomb WH, Turner AK, Jeffery N, Elliott S (2015) CICE: the Los Alamos sea ice model documentation and software user's manual version 5.1 Tech Rep LA-CC-06-012, Los Alamos National Laboratory, Los Alamos
- Hurrell JW, Holland MM, Gent PR, Ghan S, Kay JE, Kushner PJ, Lamarque JF, Large WG, Lawrence D, Lindsay K, Lipscomb WH, Long MC, Mahowald N, Marsh DR, Neale RB, Rasch P, Vavrus S, Vertenstein M, Bader D, Collins WD, Hack JJ, Kiehl J, Marshall S (2013) The community earth system model: A framework for collaborative research. *Bull Am Meteorol Soc* 94:1339–1360. doi: 10.1175/BAMS-D-12-00121.1

- Isoguchi O, Kawamura H, Oka E (2006) Quasi-stationary jets transporting surface warm waters across the transition zone between the subtropical and the subarctic gyres in the North Pacific. *J Geophys Res Ocean* 111:C10003. doi: 10.1029/2005JC003402
- Jerlov NG (1976) *Marine Optics*. Elsevier, Philadelphia, 231 pp
- Jochum M, Malanotte-Rizzoli P, Busalacchi A (2004) Tropical instability waves in the Atlantic Ocean. *Ocean Model* 7:145–163. doi: 10.1016/S1463-5003(03)00042-8
- Kalnay E, Kanamitsu M, Kistler R, Collins W, Deaven D, Gandin L, Iredell S, Saha S, White G, Woolen J, Zhu Y, Chelliah M, Ebisuzaki W, Higgins W, Janowiak J, Mo KC, Ropelewski C, Wang J, Leetmaa A, Reynolds R, Jenne R, Joseph D (1996) The NCEP/NCAR 40-year reanalysis project. *Bull Am Meteorol Soc* 77:437–471. doi: 10.1175/1520-0477(1996)077<0437:TNYRP>2.0.CO;2
- Kawai Y, Miyama T, Iizuka S, Manda A, Yoshioka MK, Katagiri S, Tachibana Y, Nakamura H (2015) Marine atmospheric boundary layer and low-level cloud responses to the Kuroshio Extension front in the early summer of 2012: Three-vessel simultaneous observations and numerical simulations. *J Oceanogr* 71:511–526. doi: 10.1007/s10872-014-0266-0
- Kelly KA, Small RJ, Samelson RM, Qiu B, Joyce TM, Kwon YO, Cronin MF (2010) Western boundary currents and frontal air-sea interaction: Gulf stream and Kuroshio Extension. *J Clim* 23:5644–5667. doi: 10.1175/2010JCLI3346.1
- Kobayashi S, Ota Y, Harada Y, Ebata A, Moriya M, Onoda H, Onogi K, Kamahori H, Kobayashi C, Endo H, Miyaoka K, Takahashi K (2015) The JRA-55 reanalysis: General specifications and basic characteristics. *J Meteorol Soc Japan* 93:5–48. doi: 10.2151/jmsj.2015-001

- Konda M, Ichikawa H, Tomita H, Cronin MF (2010) Surface heat flux variations across the Kuroshio Extension as observed by surface flux buoys. *J Clim* 23:5206–5221. doi: 10.1175/2010jcli3391.1
- Kraus EB, Turner JS (1967) A one-dimensional model of the seasonal thermocline II. The general theory and its consequences. *Tellus* 19: 98–106. doi: 10.3402/tellusa.v19i1.9753
- Kubota M, Iwasaka N, Kizu S, Konda M, Kutsuwada K (2002) Japanese ocean flux data sets with use of remote sensing observations (J-OFURO). *J Oceanogr* 58:213–225. doi: 10.1023/A:1015845321836
- Kushnir Y, Robinson WA, Bladé I, Hall NMJ, Peng S, Sutton R (2002) Atmospheric GCM response to extratropical SST anomalies: Synthesis and evaluation. *J Clim* 15:2233–2256. doi: 10.1175/1520-0442(2002)015<2233:AGRTE>2.0.CO;2
- Kwon Y-O, Alexander MA, Bond NA, Frankignoul C, Nakamura H, Qiu B, Thompson LA (2010) Role of the Gulf Stream and Kuroshio–Oyashio systems in large-scale atmosphere–ocean interaction: A review. *J Clim* 23:3249–3281. doi: 10.1175/2010JCLI3343.1
- Lawrence DM, Oleson KW, Flanner MG, Thornton PE, Swenson SC, Lawrence PJ, Zeng X, Yang Z-L, Levis S, Sakaguchi K, Bonan GB, Slater AG (2011) Parameterization improvements and functional and structural advances in version 4 of the Community Land Model. *J Adv Model Earth Syst* 3:1–27. doi: 10.1029/2011MS000045
- Legeckis (1977) Long waves in the eastern equatorial Pacific Ocean: A view from a geostationary satellite. *Science* 197:1179–1181. doi: 10.1126/science.197.4309.1179

- Lindzen RS, Nigam S (1987) On the role of sea surface temperature gradients in forcing low-level winds and convergence in the tropics. *J Atmos Sci* 44:2418–2436. doi: 10.1175/1520-0469(1987)044<2418:OTROSS>2.0.CO;2
- Lutjeharms JRE (2006) *The Agulhas Current*. Springer, New York, 329 pp
- Lutjeharms JRE, Ansorge IJ (2001) The Agulhas Return Current. *J Mar Syst* 30:115–138. doi: 10.1016/S0924-7963(01)00041-0
- MacVean MK, Woods JD (1980) Redistribution of scalars during upper ocean frontogenesis: A numerical model. *Quart J Roy Meteor Soc* 106:293–311. doi: 10.1002/qj.49710644805
- Masunaga R, Nakamura H, Miyasaka T, Nishii K, Qiu B (2016) Interannual modulations of oceanic imprints on the wintertime atmospheric boundary layer under the changing dynamical regimes of the Kuroshio Extension. *J Clim* 29:3273–3296. doi: 10.1175/JCLI-D-15-0545.1
- Masunaga R, Nakamura H, Miyasaka T, Nishii K, Tanimoto Y (2015) Separation of climatological imprints of the Kuroshio Extension and Oyashio fronts on the wintertime atmospheric boundary layer: Their sensitivity to SST resolution prescribed for atmospheric reanalysis. *J Clim* 28:1764–1787. doi: 10.1175/JCLI-D-14-00314.1
- McPhaden MJ (1995) The tropical atmosphere ocean (TAO) array is completed. *Bull Am Meteorol Soc* 76: 739–741
- Miller AJ, Cayan DR, Barnett TP, Graham NE, Oberhuber JM (1994) Interdecadal variability of the Pacific Ocean: Model response to observed heat flux and wind stress anomalies. *Clim Dyn* 9:287–302. doi: 10.1007/BF00204744
- Minobe S, Kuwano-Yoshida A, Komori N, Xie S-P, Small RJ (2008) Influence of the

- Gulf Stream on the troposphere. *Nature* 452:206–209. doi: 10.1038/nature06690
- Minobe S, Miyashita M, Kuwano-Yoshida A, Tokinaga H, Xie S-P (2010) Atmospheric response to the Gulf Stream: Seasonal variations. *J Clim* 23:3699–3719. doi: 10.1175/2010JCLI3359.1
- Miyasaka T, Nakamura H (2010) Structure and mechanisms of the Southern Hemisphere summertime subtropical anticyclones. *J Clim* 23:2115–2130. doi: 10.1175/2009JCLI3008.1
- Moisan JR, Niiler PP (1998) The seasonal heat budget of the North Pacific: Net heat flux and heat storage rates (1950–1990). *J Phys Oceanogr* 28:401–421. doi: 10.1175/1520-0485(1998)028<0401:TSHBOT>2.0.CO;2
- Morioka Y, Takaya K, Behera SK, Masumoto Y (2015) Local SST impacts on the summertime Mascarene High variability. *J Clim* 28:678–694. doi: 10.1175/JCLI-D-14-00133.1
- Morioka Y, Tozuka T, Masson S, Terray P, Luo J-J, Yamagata T (2012) Subtropical dipole modes simulated in a coupled general circulation model. *J Clim* 25:4029–4047. doi: 10.1175/JCLI-D-11-00396.1
- Morioka Y, Tozuka T, Yamagata T (2010) Climate variability in the southern Indian Ocean as revealed by self-organizing maps. *Clim Dyn* 35:1059–1072. doi: 10.1007/s00382-010-0843-x
- Morioka Y, Tozuka T, Yamagata T (2013) How is the Indian Ocean subtropical dipole excited? *Clim Dyn* 41:1955–1968. doi: 10.1007/s00382-012-1584-9
- Nakamura H, Sampe T, Goto A, Ohfuchi W, Xie S-P (2008) On the importance of midlatitude oceanic frontal zones for the mean state and dominant variability in the tropospheric circulation. *Geophys Res Lett* 35:L15709. doi:

10.1029/2008GL034010

Nakamura H, Shimpo A (2004) Seasonal variations in the Southern Hemisphere storm tracks and jet streams as revealed in a reanalysis dataset. *J Clim* 17:1828–1844. doi: 10.1175/1520-0442(2004)017<1828:SVITSH>2.0.CO;2

Nakamura M (2012) Impacts of SST anomalies in the Agulhas Current system on the regional climate variability. *J Clim* 25:1213–1229. doi: 10.1175/JCLI-D-11-00088.1

Neale RB, Chen C-C, Gettelman A, Lauritzen PH, Park S, Williamson DL, Conley AJ, Garcia R, Kinnison D, Lamarque J-F, March D, Mills M, Smith AK, Tilmes S, Vitt F, Morrison H, Camerson-Smith P, Collins WD, Iacono MJ, Easter RC, Ghan SJ, Liu X, Rasch PJ, Taylor MA (2010) Description of the NCAR community atmosphere model (CAM 5.0). NCAR Tech Note NCAR/TN-486+STR

Niiler PP, Kraus EB (1977) One-dimensional models of the upper ocean. In: Graus EB (ed) *Modelling and prediction of the upper layers of the ocean*. Pergamon Press, Oxford, pp 143–172

Nonaka M, Nakamura H, Taguchi B, Komori N, Kuwano-Yoshida A, Takaya K (2009) Air–sea heat exchanges characteristic of a prominent midlatitude oceanic front in the South Indian Ocean as simulated in a high-resolution coupled GCM. *J Clim* 22:6515–6535. doi: 10.1175/2009JCLI2960.1

Nonaka M, Xie S-P (2003) Covariations of sea surface temperature and wind over the Kuroshio and its extension: Evidence for ocean-to-atmosphere feedback. *J Clim* 16:1404–1413. doi: 10.1175/1520-0442(2003)16<1404:COSSTA>2.0.CO;2

O’Neill LW, Chelton DB, Esbensen SK (2010) The effects of SST-induced surface wind speed and direction gradients on midlatitude surface vorticity and divergence.

- J Clim 23:255–281. doi: 10.1175/2009JCLI2613.1
- O’Neill LW, Chelton DB, Esbensen SK, Wentz FJ (2005) High-resolution satellite measurements of the atmospheric boundary layer response to SST variations along the Agulhas Return Current. J Clim 18:2706–2723. doi: 10.1175/JCLI3415.1
- Ogawa F, Nakamura H, Nishii K, Miyasaka T, Kuwano-Yoshida A (2012) Dependence of the climatological axial latitudes of the tropospheric westerlies and storm tracks on the latitude of an extratropical oceanic front. Geophys Res Lett 39:L05804. doi: 10.1029/2011GL049922
- Ohishi S, Sugimoto S, Hanawa K (2015) Zonal movement of the Mascarene High in austral summer. Clim Dyn 45:1739–1745. doi: 10.1007/s00382-014-2427-7
- Oka E, Qiu B (2012) Progress of North Pacific mode water research in the past decade. J Oceanogr 68:5–20. doi: 10.1007/s10872-011-0032-5
- Paulson CA, Simpson JJ (1977) Irradiance measurements in the upper ocean. J Phys Oceanogr 7:952–956. doi: 10.1175/1520-0485(1977)007<0952:IMITUO>2.0.CO;2
- Pollard RT, Regier LA (1992) Vorticity and vertical circulation at an ocean front. J Phys Oceanogr 22:609–625. doi: 10.1175/1520-0485(1992)022<0609:VAVCAA>2.0.CO;2
- Qiu B, Chen S (2005) Variability of the Kuroshio Extension jet, recirculation gyre, and mesoscale eddies on decadal time scales. J Phys Oceanogr 35:2090–2103. doi: 10.1175/JPO2807.1
- Qiu B, Chen S (2006) Decadal variability in the formation of the North Pacific subtropical Mode Water: Oceanic versus atmospheric control. J Phys Oceanogr 36:1365–1380. doi: 10.1175/JPO2918.1

- Qiu B, Kelly KA (1993) Upper-ocean heat balance in the Kuroshio Extension region. *J Phys Oceanogr* 23:2027–2041. doi: 10.1175/1520-0485(1993)023<2027:UOHBIT>2.0.CO;2
- Reynolds RW, Smith TM, Liu C, Chelton DB, Casey KS, Schlax MG (2007) Daily high-resolution-blended analyses for sea surface temperature. *J Clim* 20:5473–5496. doi: 10.1175/2007JCLI1824.1
- Sallée J-B, Shuckburgh E, Bruneau N, Meijers AJS, Bracegirdle TJ, Wang Z (2013) Assessment of Southern Ocean mixed-layer depths in CMIP5 models: Historical bias and forcing response. *J Geophys Res Ocean* 118:1845–1862. doi: 10.1002/jgrc.20157
- Samelson RM (1993) Linear instability of a mixed-layer front. *J Geophys Res* 98:10195–10204. doi: 10.1029/93JC00457
- Samelson RM, Chapman DC (1995) Evolution of the instability of a mixed-layer front. *J Geophys Res* 100:6743–6759. doi: 10.1029/94JC03216
- Sampe T, Nakamura H, Goto A (2013) Potential influence of a midlatitude oceanic frontal zone on the annular variability in the extratropical atmosphere as revealed by aqua-planet experiments. *J Meteorol Soc Japan* 91A:243–267. doi: 10.2151/jmsj.2013-A09
- Sampe T, Nakamura H, Goto A, Ohfuchi W (2010) Significance of a midlatitude SST frontal zone in the formation of a storm track and an eddy-driven westerly jet. *J Clim* 23:1793–1814. doi: 10.1175/2009JCLI3163.1
- Saraceno M, Provost C, Piola AR, Bava J, Gagliardini A (2004) Brazil Malvinas frontal system as seen from 9 years of advanced very high resolution radiometer data. *J Geophys Res* 109:C05027. doi: 10.1029/2003JC002127

- Schmidtko S, Johnson GC, Lyman JM (2013) MIMOC: A global monthly isopycnal upper-ocean climatology with mixed layers. *J Geophys Res Ocean* 118:1658–1672. doi: 10.1002/jgrc.20122
- Shimada T, Minobe S (2011) Global analysis of the pressure adjustment mechanism over sea surface temperature fronts using AIRS/Aqua data. *Geophys Res Lett* 38:L06704. doi: 10.1029/2010GL046625
- Small RJ, Bacmeister J, Bailey D, Baker A, Bishop S, Bryan F, Caron J, Dennis J, Gent P, Hsu H-M, Jochum M, Lawrence D, Munoz E, diNezio P, Scheitlin T, Tomas R, Tribbia J, Tseng Y-H, Vertenstein M (2014) A new synoptic scale resolving global climate simulation using the community earth system model. *J Adv Model Earth Syst* 6:1065–1094. doi: 10.1002/2014MS000363
- Smith TM, Reynolds RW, Peterson TC, Lawrimore J (2008) Improvements to NOAA's historical merged land–ocean surface temperature analysis (1880–2006). *J Clim* 21:2283–2296. doi: 10.1175/2007JCLI2100.1
- Smith R, Jones P, Briegleb B, Bryan F, Danabasoglu G, Dennis J, Dukowicz J, Eden C, Fox-Kemper B, Gent P, Hecht M, Jayne S, Jochum M, Large W, Lindsay K, Maltrud M, Norton N, Peacock S, Vertenstein M, Yeager S (2010) The parallel ocean program (POP) reference manual. Tech Rep LAUR-10-01853
- Spall MA (1995) Frontogenesis, subduction, and cross-front exchange at upper ocean fronts. *J Geophys Res* 100:2543–2557. doi: 10.1029/94JC02860
- Sugimoto S, Kako S (2016) Decadal variation in winter mixed layer depth south of the Kuroshio Extension and its influence on winter mixed layer temperature. *J Clim* 29:1237–1252. doi: 10.1175/JCLI-D-15-0206.1
- Suzuki R, Behera SK, Iizuka S, Yamagata T (2004) Indian Ocean subtropical dipole

- simulated using a coupled general circulation model. *J Geophys Res* 109:C09001.
doi: 10.1029/2003JC001974
- Sverdrup HU (1947) Wind-driven currents in a baroclinic ocean; with application to the equatorial currents of the eastern Pacific. *Proc Nat Acad Sci USA* 33:318–326. doi: 10.1073/pnas.33.11.318
- Takatama K, Minobe S, Inatsu M, Small RJ (2012) Diagnostics for near-surface wind convergence/divergence response to the Gulf Stream in a regional atmospheric model. *Atmos Sci Lett* 13:16–21. doi: 10.1002/asl.355
- Takatama K, Minobe S, Inatsu M, Small RJ (2015) Diagnostics for near-surface wind response to the Gulf Stream in a regional atmospheric model. *J Clim* 28:238–255. doi: 10.1175/JCLI-D-13-00668.1
- Thompson LA (2000) Ekman layers and two-dimensional frontogenesis in the upper ocean. *J Geophys Res Ocean* 105:6437–6451. doi: 10.1029/1999JC900336
- Tokinaga H, Tanimoto Y, Xie S-P (2005) SST-induced surface wind variations over the Brazil-Malvinas confluence: Satellite and in situ observations. *J Clim* 18:3470–3482. doi: 10.1175/JCLI3485.1
- Toyoda T, Fujii Y, Kuragano T, Kamachi M, Ishikawa Y, Masuda S, Sato K, Awaji T, Hernandez F, Ferry N, Guinehut S, Martin MJ, Peterson KA, Good SA, Valdivieso M, Haines K, Storto A, Masina S, Köhl A, Zuo H, Balmaseda M, Yin Y, Shi L, Alves O, Smith G, Chang Y-S, Vernieres G, Wang X, Forget G, Heimbach P, Wang O, Fukumori I, Lee T (2015) Intercomparison and validation of the mixed layer depth fields of global ocean syntheses. *Clim Dyn*. doi: 10.1007/s00382-015-2637-7
- Tozuka T, Cronin MF (2014) Role of mixed layer depth in surface frontogenesis: The

- Agulhas Return Current front. *Geophys Res Lett* 41:2447–2453. doi:
10.1002/2014GL059624
- Tozuka T, Cronin MF, Tomita H. Surface frontogenesis by surface heat fluxes in the Kuroshio Extension region. *Sci Rep* in revision
- Tsubouchi T, Suga T, Hanawa K (2010) Indian Ocean subtropical Mode Water: its water characteristics and spatial distribution. *Ocean Sci* 6:41–50
- Wallace JM, Mitchell TP, Deser C (1989) The influence of sea-surface temperature on surface wind in the eastern equatorial Pacific: Seasonal and interannual variability. *J Clim* 2:1492–1499. doi: 10.1175/1520-0442(1989)002<1492:TIOSST>2.0.CO;2
- Wang D-P (1993) Model of frontogenesis: Subduction and upwelling. *J Mar Res* 51:497–513. doi: 10.1357/0022240933224034
- Watanabe M, Hibiya T (2013) Assessment of mixed layer models embedded in an ocean general circulation model. *J Oceanogr* 69:329–338. doi:
10.1007/s10872-013-0176-6
- Waterman S, Hoskins BJ (2013) Eddy shape, orientation, propagation, and mean flow feedback in western boundary current jets. *J Phys Oceanogr* 43:1666–1690. doi:
10.1175/JPO-D-12-0152.1
- Waterman S, Jayne SR (2011) Eddy-mean flow interactions in the along-stream development of a western boundary current jet: An idealized model study. *J Phys Oceanogr* 41:682–707. doi: 10.1175/2010JPO4477.1
- Weller RA (1991) Overview of the frontal air-sea interaction experiment (FASINEX): A study of air-sea interaction in a region of strong oceanic gradients. *J Geophys Res* 96:8501–8516. doi: 10.1029/90JC01868
- Willett CS, Leben RR, Lavín MF (2006) Eddies and tropical instability waves in the

- eastern tropical Pacific: A review. *Prog Oceanogr* 69:218–238. doi:
10.1016/j.pocean.2006.03.010
- Williams RG, Wilson C, Hughes CW (2007) Ocean and Atmosphere Storm Tracks: The Role of Eddy Vorticity Forcing. *J Phys Oceanogr* 37:2267–2289. doi:
10.1175/JPO3120.1
- Xie S-P (2004) Satellite observations of cool ocean–atmosphere interaction. *Bull Am Meteorol Soc* 85:195–208. doi: 10.1175/BAMS-85-2-195
- Xie S-P, Ishiwatari M, Hashizume H, Takeuchi K (1998) Coupled ocean-atmospheric waves on the equatorial front. *Geophys Res Lett* 25:3863–3866. doi:
10.1029/1998GL900014
- Yasuda I, Tozuka T, Noto M, Kouketsu S (2000) Heat balance and regime shifts of the mixed layer in the Kuroshio Extension. *Prog Oceanogr* 47:257–278. doi:
10.1016/S0079-6611(00)00038-0
- Yasuda T, Hanawa K (1997) Decadal changes in the Mode Waters in the midlatitude North Pacific. *J Phys Oceanogr* 27:858–870. doi:
10.1175/1520-0485(1997)027<0858:DCITMW>2.0.CO;2
- Yu J-Y, Liu WT (2003) A linear relationship between ENSO intensity and tropical instability wave activity in the eastern Pacific Ocean. *Geophys Res Lett* 30:1735. doi: 10.1029/2003GL017176
- Yu L, Weller RA (2007) Objectively analyzed air–sea heat fluxes for the global ice-free oceans (1981–2005). *Bull Am Meteorol Soc* 88:527–539. doi:
10.1175/BAMS-88-4-527